

## CALCIUM CARBONATE BASED POROUS MEDIA

IMPROVING CALCIUM CARBONATE BASED POROUS MEDIA FOR LATERAL  
FLOW ASSAYS

By ALEXANDRA SZEWCZYK, B.ENG. BIOSCI.

A Thesis Submitted to the School of Graduate Studies in Partial Fulfilment of the  
Requirements for the Degree Master of Applied Science

McMaster University © Copyright by Alexandra Szewczyk, August 2020

McMaster University MASTER OF APPLIED SCIENCE (2020) Hamilton, Ontario  
(Chemical Engineering)

TITLE: Improving Calcium Carbonate Based Porous Media for Lateral Flow Assays  
AUTHOR: Alexandra Szewczyk B.Eng.Biosci. (McMaster University) SUPERVISORS:  
Professor C.D.M. Filipe, Professor R. Pelton NUMBER OF PAGES XI, 57

## ABSTRACT

Nitrocellulose is currently the most common porous material used in commercially available lateral flow assays. It is, however, unsafe to manufacture and time consuming to incorporate into multi-component assay devices. Precipitated calcium carbonate is a material produced from naturally occurring lime that can be suspended in a binder and extruded onto a surface. This extruded suspension forms a porous coating through which a solution can be wicked. The physical characteristics of three different types of calcium carbonate types were investigated to determine differences that may yield better lateral flow. The capillary flow rate through the coating was found to be largely affected by the calcium carbonate type used, the binder concentration and whether any post-printing treatment was applied, specifically heating the print. Calcium carbonate has a high specific surface area, which results in a high protein binding capacity. To prevent protein binding, pre-treating calcium carbonate particles prior to forming the suspension in a binder was attempted. Pre-treatment with bovine serum albumin, casein or methoxy-PEG phosphate did not show prevention of protein binding. Furthermore, by treating the calcium carbonate particles with a protein before suspension formulation, the wicking rate after printing was found to be diminished.

## ACKNOWLEDGEMENTS

I want to thank my supervisors Dr. Robert Pelton and Dr. Carlos Filipe who throughout my masters provided enormous support, and a breadth of technical expertise that I applied at every step of this journey. I further want to thank Dr. Zela Li who introduced me to the topic of calcium carbonate based lateral flow assays and who forged the path that I had the privilege of following. I also had the opportunity to learn from numerous experts in the field of interfacial engineering including Dr. Marta Prinz, Dr. Mehdi Keramane, and Dr. Dan Chen, and for their knowledge I am grateful.

I want to extend my thanks to NSERC for the Canada Graduate Scholarship that provided me with the financial security to complete my program. Many talented and ambitious individuals are unable to pursue higher education because of financial setbacks and I thoroughly recognize the gift that I was given when I received this scholarship.

Beyond those who directly worked on this project with me, I want to thank the individuals who supported me outside of the lab. To Steven Myers, Melissa Larocque, Logan Groves, Abhishek Premachandra, Cassandra Chidiac and Aakash Shaw, thank you for your friendship and understanding. To my mother, thank you for your constant encouragement.

Lastly, I would like to sincerely thank Dr. Vincent Leung and, again, Dr. Carlos Filipe, for introducing me to research in chemical engineering when I was completing my undergraduate studies. It has opened countless doors for me and continues to do so.

## CONTENTS

1	Introduction.....	1
1.1	Motivation for Lateral Flow Assays .....	1
1.2	Function of Lateral Flow Assays .....	2
1.3	Defining Objectives and Metrics for Lateral Flow Assays.....	3
1.4	Physical Theories of Lateral Flow Assays.....	6
1.5	Current Materials Used for Lateral Flow Assays.....	8
1.6	Properties of Nitrocellulose Manufactured for LFAs .....	8
1.7	Limitations of Currently Available Lateral Flow Assays .....	14
1.8	Alternative 3D Printed Porous Media.....	16
1.9	Printable Calcium Carbonate as an Alternative Material to Nitrocellulose 20	
1.10	Material Properties of Calcium Carbonate .....	21
1.11	Objectives .....	22
2	Methods .....	24
2.1	Evaluation of the Properties of Precipitated Calcium Carbonate .....	24
2.1.1	Experimental Design.....	24
2.1.2	Materials .....	24
2.1.3	Experimental Methods .....	25
2.2	Ink Formulation Factors Affecting Wicking Rate .....	25
2.2.1	Experimental Design.....	25
2.2.2	Materials .....	27
2.2.3	Experimental Methods .....	27
2.3	Blocking Protein Adsorption to Calcium Carbonate in Solution.....	29
2.3.1	Experimental Design.....	29
2.3.2	Materials .....	29
2.3.3	Experimental Methods .....	30
2.4	Wicking Tests with Blocked Calcium Carbonate .....	31
2.4.1	Experimental Design.....	31
2.4.2	Materials .....	31
2.4.3	Experimental Methods .....	32
3	Results and Discussion .....	32
3.1	Evaluation of the Properties of Precipitated Calcium Carbonate .....	32
3.2	Ink Formulation Factors Affecting Wicking Rate .....	34
3.2.1	DOE Investigating the Effect of Ink Composition on Wicking Rate .....	34
3.2.2	Effect of Heating Print on Wicking Rate.....	38
3.2.3	Effect of Combining Calcium Carbonate Types on Wicking Rate.....	40
3.2.4	Image Analysis of Printed Ink .....	41
3.3	Blocking Calcium Carbonate in Solution .....	44
3.3.1	Casein Blocking .....	44
3.3.2	BSA Blocking .....	47
3.3.3	Phosphorylated PEG Blocking .....	49
3.4	Wicking Rate of Coatings Composed of Blocked Calcium Carbonate ...	52

4	Conclusion.....	53
4.1	Summary of Results.....	53
4.2	Comparing Calcium Carbonate Based Media to Other 3D Printing Forms 55	
5	References.....	58

## LIST OF FIGURES

Figure 1. General structure of a commercially available lateral flow assay. Reproduced from [5]. Dashed lines indicate optional housing of the lateral flow assay unit. Blue arrow indicates direction of flow from the sample pad to absorbent pad. ....	3
Figure 2. Analyte flux balance over the reaction line of a lateral flow assay. Reproduced from [12]. ....	7
Figure 3. Biodot XYZ3060 Dispenser extruding calcium carbonate ink onto glass microscope slide.....	28
Figure 4. Schematic of a printed glass slide sample set up for a vertical wicking rate test. ....	29
Figure 5. Magnification of (a) LPCC, (b) MCC 75, (c) MCC 100 particles in 1mM NaHCO <sub>3</sub> . A magnification level of 40× was used in all images. Red scale bars indicate 40 μm in the image.....	33
Figure 6. Pareto plot showing the absolute value of the effects of binder concentration, B, calcium carbonate type, P, and calcium carbonate concentration, C. Interaction of the effects is also shown. An α value of 0.05 was used in the analysis. ....	35
Figure 7. Difference between wicking rates of printed ink heated at 90°C for 5 minutes compared to non-heated. Prints were composed of light PCC. ....	39
Figure 8. Wicking rates of inks consisting of mixes of calcium carbonate types in comparison to inks of only one calcium carbonate type.....	40
Figure 9. Imaging areas of a printed ink sample with respect to its location on the microscope slide. A typical print sample has three lanes printed, with the focus of the microscope images being on one of the three. Area 1 shows one edge of the print, area 2 shows the center, and area 3 shows the opposite edge.....	42
Figure 10. Magnified images of printed ink consisting of (i)15 wt% LPCC, or (ii) 15 wt% MCC 75, with 1.12 wt% latex binder. Image (a), (b), and (c) correspond to areas 1, 2, 3 indicated in Figure 9. Images taken at 4× magnification level. Red scale bars indicate 400 μm in the image.....	43
Figure 11. Magnified images of printed (a)15 wt% LPCC, (b) 15 wt% MCC 75, with 1.12 wt% latex binder. Images were taken at 40× magnification level. Red scale bars indicate 40 μm in the image.....	44

Figure 12. Comparison of adsorbed fraction of ALP on calcium carbonate particles that have and have not undergone casein pre-treatment. Experiments were performed on three calcium carbonate types: LPCC (black), MCC 75 (grey), MCC 100 (blue). .....	46
Figure 13. Comparison of adsorbed fraction of ALP on calcium carbonate particles that have and have not undergone BSA pre-treatment. Experiments were performed on three calcium carbonate types: LPCC (black), MCC 75 (grey), MCC 100 (blue). .....	48
Figure 14. Comparison of adsorbed fraction of ALP on calcium carbonate particles that have and have not undergone PEG-P pre-treatment. Experiments were performed on three calcium carbonate types: LPCC (black), MCC 75 (grey), MCC 100 (blue). .....	50
Figure 15. Chemical structure of methoxy PEG phosphate. Recreated using PubChem Sketcher V2.4 from [93]. .....	51
Figure 16. Wicking distance at 1 minute (green), 2 minutes (red), 5 minutes (blue) in prints containing calcium carbonate pre-treated with BSA compared to non-pre-treated calcium carbonate. ....	53

## LIST OF TABLES

Table 1. Objectives of lateral flow assays and metrics to determine whether they were achieved. ....	5
Table 2. Manufacturer specifications for nitrocellulose membranes designed for lateral flow assays as provided by product specification sheets. ....	13
Table 3. Examples of research into 3D Printing of Porous Media .....	19
Table 4. Conditions for the 3-factor, 2-level DOE investigating ink formulation on wicking rate.....	26
Table 5. Properties of light PCC, MCC 75 and MCC 100. Specific surface area (SSA) was determined using BET method, the pore volume and half-pore width were measured using DFT method and particle size distribution was measured using MIE theory method.....	32
Table 6. DOE summary and results for the investigation of ink composition on wicking rate. The factors investigated include binder concentration, B, PCC concentration, C, type of PCC, P. Actual run refers to the order in which the experiment was performed and the Design Run refers to the order in which the experiment was designed.....	35
Table 7. DOE model coefficients and P-values for analysis of term significance.....	35
Table 8. Weighted Pugh matrix comparing porous membranes: NC (nitrocellulose), C (cellulose/paper [13]), PCC (precipitated calcium carbonate), 3D-1 (Material extrusion of ink composed of sacrificial templates with silica (refer to Table 3)), 3D-2 (Multi-directional UV lithography using OFSE (refer to Table 3)). ....	56

## LIST OF ABBREVIATIONS AND SYMBOLS

GCC	Ground Calcium Carbonate
PCC	Precipitated Calcium Carbonate
MCC	Modified Calcium Carbonate
LFA	Lateral Flow Assay
ALP	Alkaline Phosphatase
BSA	Bovine Serum Albumin

## DECLARATION OF ACADEMIC ACHIEVEMENT

This is a declaration that the entirety of this report was written by Alexandra Szewczyk. The performance of experiments and data analysis was performed by Alexandra Szewczyk. Dr. Filipe and Dr. Pelton provided technical guidance and suggestions as to what experiments should be performed. Dr. Zela Li published a paper and included a chapter of her thesis on the subject which was the basis of this work. Many of the experimental set-ups used in this work were designed and physically constructed by Dr. Zela Li.

# 1 INTRODUCTION

## 1.1 Motivation for Lateral Flow Assays

Obtaining analytical laboratory results without the wait-time and non-mobile nature associated with traditional laboratory testing methods is advantageous in many fields of study, including water quality control, medical sample analysis, and food science. In particular, point-of-care medical testing is rapidly gaining interest, whereby medical tests are performed outside of a typical medical services facility [1]. Point-of-care diagnostic tools are a means of minimizing test time and testing in situations/environments that lack standard medical diagnostic equipment. Additionally, point-of-care testing can provide efficient and direct information to individuals who depend on frequent monitoring of a condition. In a 2017 study of service readiness of 8443 health facilities in 10 developing countries, only 2% were found to provide access to basic diagnostic tests [2]. For this reason, more must be done to make diagnostic assays readily accessible and dependable. The World Health Organization has defined the benchmark characteristics for ideal diagnostic tests in areas with limited medical resources, as being: (1) affordable, (2) sensitive, (3) specific, (4) user-friendly, (5) rapid and robust, (6) equipment-free, and (7) deliverable to end users (ASSURED) [3]. Lateral flow assays (LFAs) offer a mechanism for point-of-care testing that satisfies all ASSURED characteristics.

Since the late 1960s, LFAs have been used for diagnostic testing [4]. The most recognizable commercially available LFAs are used to detect human chorionic gonadotropin (hCG) in urine for pregnancy testing [5]. There are, however, other LFA products on the market that are designed to detect infectious diseases (for example, malaria,

HIV, tuberculosis, legionnaire's disease, and influenza), cancers (for example, bladder, cervical, and colon cancer), cardiac diseases (for example, myocardial infarction), and drugs [4].

## **1.2 Function of Lateral Flow Assays**

Lateral flow assays (LFA) are a type of assay characterized by the wicking of a sample through a porous medium which facilitates chromatographic separation and immunochemical reaction [4]. A typical antibody-based sandwich LFA consists of a sample pad, which may contain buffer salts and surfactants, onto which a liquid sample is added [5], [6]. The sample pad leads to a conjugate pad containing stabilized detector particles (for example, gold nanoparticles, latex beads, or quantum dots) complexed with an antibody that binds with the analyte-of-interest in the sample solution as it wicks through the conjugate pad [4], [5]. Then, travelling through the porous medium, the sample reaches a capture reagent line where it binds to a second immobilized antibody, producing a line of concentrated colour which indicates the presence of the analyte [4]. Most assays are designed with a control line downstream from the test line containing a third immobilized antibody, which binds to any antibody from the conjugate pad that does not have bound analyte [4]. At the end of the flow path is an absorbent pad that allows wicking to be maintained and collects residual sample [4]. Figure 1 shows the structure of a typical lateral flow assay. In addition to the sandwich assay format, there are other non-competitive and competitive assay formats with different binding sequences and result display [4].

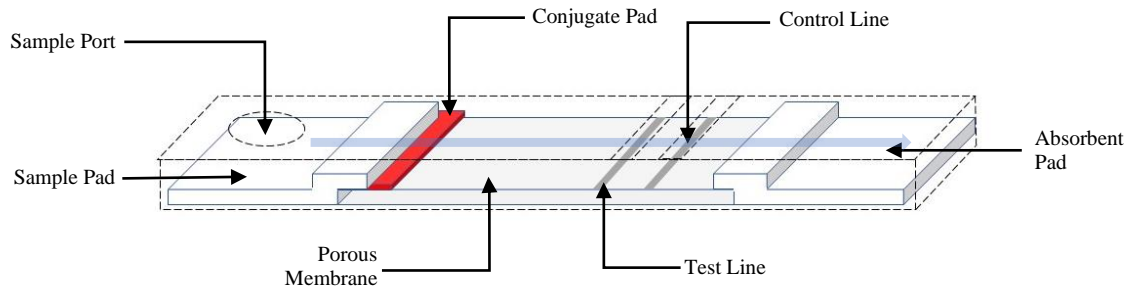


Figure 1. General structure of a commercially available lateral flow assay. Reproduced from [5]. Dashed lines indicate optional housing of the lateral flow assay unit. Blue arrow indicates direction of flow from the sample pad to absorbent pad.

### 1.3 Defining Objectives and Metrics for Lateral Flow Assay Materials

Lateral flow assays are diverse in the target analyte they capture and how they report results, but it is important to define the common design elements that they must meet. This enables the objective selection of prospective materials and different assay formats for specific applications. Firstly, LFAs, and, in turn, the materials that they are composed of, must meet the ASSURED objectives outlined by the WHO. These objectives provide a basis of general goals any diagnostic tool, specifically medical related, should be designed to achieve. Other criteria including material specifications, and manufacturability requirements that specifically apply to lateral flow assay materials must also be defined [3], [5], [7]–[9].

Table 1 summarizes overall metrics for assessing lateral flow assay materials. These metrics are grouped into six categories of objectives including: (1) Controllable Flow Dynamics, (2) Controllable and Predictable Assay Interactions, (3) Mechanical Durability, (4) Chemical Durability, (5) Ease of Manufacturability, (6) Ease of Use. This grouping structure allows for a clear understanding of how each metric plays a role in LFA

production and function and what aspect of the design is affected when a metric is not achieved. Most of the ASSURED metrics fall into the second and sixth objectives, focusing on having a high performing sensitive and selective assay, with low end user cost.

Many of these metrics cannot be satisfied without consideration of other metrics. This is because there are key factors that influence multiple metrics. For example, high sensitivity and specific capillary flow rate both depend on pore characteristics and chemistry. Sometimes these key factors are beneficial for one metric and not another, for example, improving wettability of a porous media may increase the capillary flow rate, but consequently may decrease the amount of protein binding due to fewer sites for hydrophobic interactions to occur.

Table 1. Objectives of lateral flow assays and metrics to determine whether they were achieved.

<b>Objectives</b>	<b>Metric</b>	<b>Key Factors</b>	<b>Reasoning</b>
Controllable Flow Dynamics	<ol style="list-style-type: none"> <li>1. Large range of capillary flow rates</li> <li>2. Selectable specific capillary flow rate</li> <li>3. Uniform wicking front</li> </ol>	<ol style="list-style-type: none"> <li>i. Pore size</li> <li>ii. Pore size distribution</li> <li>iii. Porosity</li> <li>iv. Wettability</li> <li>v. Porous media chemistry</li> <li>vi. Manufacturing technology resolution, precision, accuracy</li> </ol>	The flow through a lateral flow assay determines the time duration of sample separation and reaction. Different applications require different capillary flow rates.
Controllable and Predictable Assay Interactions	<ol style="list-style-type: none"> <li>1. High protein binding capacity</li> <li>2. Effective protein blocking</li> <li>3. Correct protein orientation</li> <li>4. Retention of protein activity</li> <li>5. Specific to the analyte of interest</li> <li>6. Sensitive to low concentrations of analyte of interest</li> <li>7. Modifiable surface chemistry</li> </ol>	<ol style="list-style-type: none"> <li>i. Porous media chemistry</li> <li>ii. Specific surface area</li> <li>iii. Porosity</li> <li>iv. Pore size</li> <li>v. Pore size distribution</li> <li>vi. Wettability</li> </ol>	The porous media used in the assay must be able to both immobilize a high concentration of the specific antibody that binds to the target analyte and prevent the target analyte from binding in other locations.
Mechanical Durability	<ol style="list-style-type: none"> <li>1. High tensile strength</li> <li>2. Non-collapsing pores and void space</li> <li>3. Wet strength</li> </ol>	<ol style="list-style-type: none"> <li>i. Porous media chemistry</li> <li>ii. Thickness of media</li> <li>iii. Binding to manufacturing base</li> </ol>	Thin porous media allows for low sample volumes but also results in mechanical weakness. This often necessitates the use of backing support, protective casings, or extra care in handling of the assays.
Chemical Durability	<ol style="list-style-type: none"> <li>1. Low extractables/leachables</li> <li>2. Low/high pH resistance</li> <li>3. Compatible with sample polarities</li> <li>4. High temperature resistance</li> <li>5. Chemically inert</li> </ol>	<ol style="list-style-type: none"> <li>i. Porous media chemistry</li> </ol>	In manufacturing porous membranes, there cannot be remaining artifacts that interfere in assay reactions. The assay material itself also should not interfere with the assay. Furthermore, assay materials should be able to be made compatible with different sample types.
Ease of Manufacturability	<ol style="list-style-type: none"> <li>1. Low incidence of surface defects</li> <li>2. High reproducibility</li> <li>3. Choice of dimensions</li> <li>4. Low safety risk</li> </ol>	<ol style="list-style-type: none"> <li>i. Manufacturing technology resolution, precision, accuracy</li> </ol>	To be a candidate for lateral flow assays, large scale manufacturing should be possible with good lot-to-lot reproducibility and adherence to design specifications.
Ease of Use	<ol style="list-style-type: none"> <li>1. Clear display of results</li> <li>2. Minimal equipment requirements</li> <li>3. Timely results</li> <li>4. Low cost</li> </ol>	<ol style="list-style-type: none"> <li>i. Choice of detector particle</li> <li>ii. Porous media chemistry</li> <li>iii. Brightness of porous media</li> </ol>	The overarching purpose of lateral flow assays is to provide simple to interpret diagnostic test results directly to the user and limit manufacturing, labor, and equipment costs.

## 1.4 Physical Theories of Lateral Flow Assays

Lateral flow assays function by capillary pressure which enables wicking through a porous medium [10]. By balancing the forces across the meniscus of a liquid travelling through a capillary, the Young-Laplace equation can be derived to describe capillary pressure, shown in Equation 1. Given this equation, it can be concluded that capillary pressure is a function of pore radius,  $r$ , surface energy,  $\gamma$ , and contact angle,  $\theta$ .

$$P = \frac{2\gamma \cos(\theta)}{r} \quad \text{Equation 1}$$

By combining the Young-Laplace equation with the Poiseuille equation to account for viscous resistance, the Lucas-Washburn equation can be derived which relates the distance travelled by a wicking front to the wicking time, shown below in Equation 2.

$$L^2 = \left( \frac{\gamma \cos(\theta)r}{2\mu} \right) t \quad \text{Equation 2}$$

The Lucas-Washburn equation assumes that a porous media consists of uniformly sized and aligned capillary tubes and that there is complete saturation upstream from the front [10], [11]. This does not accurately describe the structure of most porous media. However, it can still be used for simple wicking flow modelling. For this reason, wicking rate is frequently reported in units of distance/time<sup>1/2</sup>.

In the design of an LFA, being able to control capillary flow rate (otherwise referred to as wicking rate) is necessary to the formation of a signal at the reaction line [5]. If  $dC_{An}/dt$  is the rate of change in analyte concentration at the reaction line, then it relates to the concentrations of the unbound analyte at the reaction line,  $C_{An}$ , unbound antibody

immobilized at the reaction line,  $C_{Anti}$ , and the bound analyte-antibody complex,  $C_{An+Anti}$ , through a binding rate constant,  $k_b$ , and unbinding constant,  $k_u$ , as seen in Equation 3 [12].

$$-\frac{dC_{An}}{dt} = k_b C_{An} C_{Anti} - k_u C_{An+Anti} \quad \text{Equation 3}$$

By increasing the flow rate through the LFA, the effective concentration of the analyte decreases due to the decrease in interaction time between the analyte and antibody [5]. This is clearly seen when doing a flux balance over the reaction line at pseudo-steady state, seen in Figure 2, which assumes velocity does not change substantially over the reaction line region [12]. This is important because velocity does change as the front moves across a porous material over a more substantial distance. Equation 4, 5, and 6 show the analyte balance across the reaction line. At early time points, it can be assumed that no analyte-antibody complexes have formed so  $C_{An+Anti} = 0$ , which allows for the simplification seen in Equation 7 [12]. In this equation, as velocity increases, the concentration of unbound analyte increases.

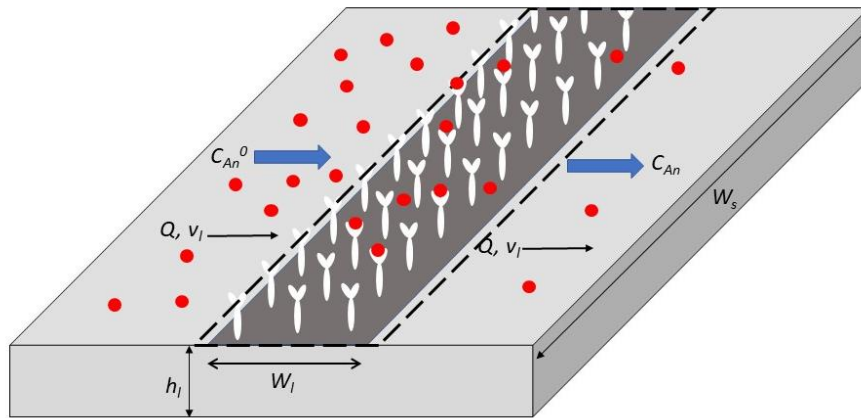


Figure 2. Analyte flux balance over the reaction line of a lateral flow assay. Reproduced from [12].

$$Q(C_{An}^0 - C_{An}) = rV_l \quad \text{Equation 4}$$

$$\left(\frac{v_l}{w_l}\right)(C_{An}^0 - C_{An}) = k_b C_{An} C_{Anti} - k_u C_{An+Anti} \quad \text{Equation 5}$$

$$C_{An} = \frac{\left(k_u C_{An+Anti} + C_{An}^0 \left(\frac{v_l}{w_l}\right)\right)}{\left((k_b C_{Anti}) + \frac{v_l}{w_l}\right)} \quad \text{Equation 6}$$

$$C_{An} = \frac{C_{An}^0}{\left(\frac{w_l}{v_l}(k_b C_{Anti}) + 1\right)} \quad \text{Equation 7}$$

At the reaction line of a LFA, analyte diffusion is typically faster than binding reactions, so the relative fluid velocity in these regions must be optimized [12].

## 1.5 Current Materials Used for Lateral Flow Assays

The material of choice for most LFAs is nitrocellulose, also known as cellulose nitrate or mixed cellulose ester. Polyvinylidene fluoride (PVDF), charge-modified nylon, cellulose and polyethersulfone (PES) are all alternative materials that have been used in place of nitrocellulose [5], [13]. These membranes differ by their primary binding mechanism (electrostatic, hydrophobic, ionic) and by the pore size, porosity, thickness, and structure [5].

## 1.6 Properties of Nitrocellulose Manufactured for LFAs

Nitrocellulose is created by reacting cellulose with nitric acid which results in the substitution of hydroxyl groups with nitrate groups, as shown in Equation 8 [5], [14].



The nitrogen content of nitrocellulose is less than the 14.14% that would occur with complete substitution of hydroxyl groups, with anything over 13.5%, being unstable [15]. Nitrocellulose membranes have a nitrogen content under 12.5%, with some references stating a typical range of 10.7% and 12.3% [16], [17]. Increasing nitrogen content in nitrocellulose decreases the decomposition temperature and, as such, any nitrocellulose product with a nitrogen content of over 12.6% is considered an explosive [17].

Nitrocellulose membranes are typically manufactured by phase inversion whereby a polymer solution separates into two phases, one polymer rich, which becomes the membrane structure upon drying, and the other polymer poor, which becomes the pores [18]. By adding anionic surfactants to nitrocellulose, the surface tension and contact angle can be manipulated to increase the wettability of the membrane [14], [19]. The material is typically cast onto a backing of non-porous film, commonly polystyrene, polyvinyl chloride, or polyester, which improves the physical strength and acts as a barrier between the membrane and any adhesives used in the assembly of an LFA [5], [7]. The thickness of the backing is selected based on whether the LFA will be stored in a protective cassette; if a cassette is to be used, only a thin backing is required [7]. Non-backed membranes are also available, however, they are more fragile and have differences in surface characteristics on the side exposed to air during casting and the side that makes contact with the casting belt [5].

To accurately predict the flow through nitrocellulose membranes, both the characteristics of the fluid and the material must be known. Accurately specifying a manufactured membrane is essential for this reason. Most manufacturers measure capillary

flow rate (wicking rate), thickness, tensile strength, surface quality, surface texture, and dimensions, and evaluate the severity of pinholes, casting lines, scratches and dents, colour, and dirt or grease from slitting, to see if they fall within acceptable quality limits [5]. Furthermore, for the purpose of application in LFAs, proteins must be able to bind to nitrocellulose so many manufacturers further specify the protein binding capacity. The mechanism of protein binding to nitrocellulose membranes as used in LFAs is still debated to be either through electrostatic interactions or hydrophobic interactions or both. Nitrate ester dipoles can interact with protein peptide bonds electrostatically [5]. Hydrophobic interactions between hydrophobic regions of a protein and the carbon-containing cellulose backbone of the nitrocellulose polymer may also occur [14].

When designing porous materials for lateral flow assays, knowing the properties of the current industry standard, nitrocellulose, is necessary in making an improved product. Specifications of nitrocellulose products marketed specifically for LFAs are shown in Table 2. All manufacturers provide data on capillary flow rate and membrane thickness, however, not all specify the pore size, tensile strength, and protein binding. Capillary flow rate is the distinguishing property among the different product types that each manufacturer produces. A specific capillary flow rate is chosen such that the test produces results within a required time frame and with high enough sensitivity, which, as previously stated in Section 0, is inversely related to capillary flow rate. Based on the manufacturer specifications observed, slower capillary flow rates tend to be associated with larger batch capillary flow variation, possibly due to difficulties in manufacturing smaller pore sizes. This may encourage

selection of a membrane with faster capillary flow and lower batch variation at the expense of decreasing binding time of the analyte.

Nitrocellulose membranes are also manufactured for protein blotting and filter applications. These nitrocellulose membranes have pore sizes smaller than those of nitrocellulose membranes designed specifically for LFAs. For example, Invitrogen manufactures filter/blotting membranes with a pore size of 0.2  $\mu\text{m}$  and 0.45  $\mu\text{m}$  which is over ten times smaller than the smallest pore size reported for MDI membranes with pore sizes of 5 to 15  $\mu\text{m}$ , seen in Table 2 [20]. Furthermore, these membranes have different protein binding capacities. Invitrogen filter/blotting nitrocellulose membranes with a pore size of 0.2  $\mu\text{m}$  and 0.45  $\mu\text{m}$  have protein binding capacities of 209 and 80  $\mu\text{g}/\text{cm}^2$  of external membrane surface area respectively, as compared to EMD Millipore LFA membranes which have protein binding capacities ranging between 50 and 120  $\mu\text{g}/\text{cm}^2$ , seen in Table 1. This difference in target pore size relates to the different functions of the membranes, blotting or lateral flow. The pore size of nitrocellulose membranes is generally inversely related to the protein binding capacity, as smaller pore sizes allow for greater surface area for protein binding [21]. Manufacturers do not include details about proprietary membrane treatment methods in product specification sheets, or any contact angle information.

Outside of commercially available membranes, some researchers study nitrocellulose properties by manufacturing their own membrane samples. Research by Ahmad et al. investigated diffusion of protein solutions through nitrocellulose membranes with five pore sizes ranging from 1.3 to 7.5  $\mu\text{m}$  produced using dry phase inversion [22], [23]. It was found that nitrocellulose membranes with a pore size of 1.3  $\mu\text{m}$  had a porosity

of 66.93% while membranes with pore sizes over 4  $\mu\text{m}$  had a porosity of over 77% [22]. Further research by the same group examined the impact of membrane thickness on porosity and pore formation. Membranes with a cast thickness of 600, 700, and 800  $\mu\text{m}$  had porosities of 77.52%, 80.04% and 80.28%, respectively, and this increase in porosity with increasing thickness also corresponded to increase in wicking rate [23]. It was also observed that macrovoids formed in membranes with a cast thickness of 800  $\mu\text{m}$  [23]. Macrovoids are pores with an elongated structure that can extend the width of a membrane and can potentially impede capillary flow [18], [24]. Another known factor in the formation of macrovoids is rapid solvent evaporation [18]. For this reason and others, the manufacturing of nitrocellulose membranes through phase inversion is highly sensitive to temperature and humidity [18].

Table 2. Manufacturer specifications for nitrocellulose membranes designed for lateral flow assays as provided by product specification sheets.

Manufacturer	Product	Manufacturer Provided Properties							Ref.
		Pore Size (µm)	Capillary Flow Rate (s/4 cm)	Capillary Flow Rate Variation	Thickness (µm)	Thickness Variation	Backed Tensile Strength (lbs/in <sup>2</sup> )	Protein Binding (µg/cm <sup>2</sup> )	
Pall	Vivid 90 LFNC	Not Available	83.4	2.5*	190-230	Not Available	Not Available	Not Available	[25]
Pall	Vivid 120 LFNC	Not Available	121.9	3.8*	190-230	Not Available	Not Available	Not Available	[25]
EMD Millipore	HF 075	Not Available	75	19**	135, 185, 235	19 µm	>10	Insulin: >50 BSA: >65 Goat IgG: >120	[26], [27]
EMD Millipore	HF 090	Not Available	90	23**	135, 185, 235	19 µm	>10	Insulin: >50 BSA: >65 Goat IgG: >120	[26], [27]
EMD Millipore	HF 120	Not Available	120	30**	135, 185, 235	19 µm	>10	Insulin: >50 BSA: >65 Goat IgG: >120	[26], [27]
EMD Millipore	HF 135	Not Available	135	34**	135, 185, 235	19 µm	>10	Insulin: >50 BSA: >65 Goat IgG: >120	[26], [27]
EMD Millipore	HF 180	Not Available	180	45**	135, 185, 235	19 µm	>10	Insulin: >50 BSA: >65 Goat IgG: >120	[26], [27]
EMD Millipore	HF 240	Not Available	240	26**	135, 185, 235	19 µm	>10	Insulin: >50 BSA: >65 Goat IgG: >120	[26], [27]
MDI *** Membrane Technology	CNPB	Not Available	70	12	110	15	Not Available	Not Available	[28]
		Not Available	90	15	110	15	Not Available	Not Available	[28]
		Not Available	150	20	110	15	Not Available	Not Available	[28]
		Not Available	200	35	110	15	Not Available	Not Available	[28]
MDI *** Membrane Technology	CNPF	5	220	25	100	15	Not Available	Not Available	[29]
		8	170	25	110	15	Not Available	Not Available	[29]
		10	125	25	100	15	Not Available	Not Available	[29]
MDI *** Membrane Technology	CNPC	10	140	28	105	15	Not Available	Not Available	[30]
		12	120	28	105	15	Not Available	Not Available	[30]
		15	100	25	105	15	Not Available	Not Available	[30]

\*Range is in terms of  $\pm\sigma$  based on three samples from a single lot (intra-lot)

\*\*Range is provided in terms of  $\pm 3\sigma$  based on an unknown number of samples from a single roll

\*\*\*Limited information provided about what kind of deviation ranges are shown

## 1.7 Limitations of Currently Available Lateral Flow Assays

As previously outlined, there are many advantages associated with lateral flow assays, including portability, ease-of-use, and rapid result delivery. There are, however, limitations to currently available lateral flow assays, including (1) what information lateral flow assays can convey, (2) the assay sensitivity and specificity, (3) the incorporation of multiplex reactions, and (4) the complexity of the manufacturing process.

Most lateral flow devices provide a visual output to qualitatively state whether an analyte is present in a sample or not. This design simplicity contributes to the low cost and ease-of-use of such devices. In many instances, this is insufficient information to deem a biosensor useful, especially in cases where medical treatment depends on the concentration of an analyte, not just the presence. There have been advancements in improving the quantitative results provided by LFAs through incorporation of measuring devices. Several research groups have developed cellphone-based technologies for imaging and analyzing the results of LFAs, most requiring a removable phone attachment with an LED and a phone application that measures light reflection or transmission [31], [32]. Digital pregnancy tests that are commercially available utilise a similar functionality. Depending on the label chosen for the assay, the accuracy of quantitative readings can be improved. Up-converting nanoparticles are one such technology being considered for this purpose [33]. Attempts at implementing electrochemical transducers that can detect the current across electrodes at the test line of a pregnancy test due to the flow of gold nanoparticles has also been considered for quantitative readings [34].

The sensitivity of an assay is defined as the proportion of disease-positive cases where a positive test result is obtained, as seen in Equation 9 [35]. The specificity of an assay is defined as the proportion of disease-negative cases where a negative test result is obtained, as seen in Equation 9 and 10 [35].

$$\text{Sensitivity} = \frac{\text{True positives}}{\text{True positives} + \text{False negatives}} \quad \text{Equation 9}$$

$$\text{Specificity} = \frac{\text{True negatives}}{\text{True negatives} + \text{False positives}} \quad \text{Equation 10}$$

An ideal biosensor has both high sensitivity and specificity. Low sensitivity can result when capillary flow rates are too high, as stated in Section 0, or the analyte/sample are not available in large concentrations/quantities [26]. In both these situations, the analyte and antibody do not have enough interaction time. Non-specific binding of the analyte of interest to the substrate before reaching the test line in an LFA can also result in low sensitivity. When non-specific binding occurs, it is typically the result of interactions caused by either hydrophobic, ionic, van der Waals forces or hydrogen bonding between the proteins and a surface that is not the intended target [36]. Low specificity occurs if multiple molecules including the analyte of interest can bind to the test line. Depending on the test being performed, nitrocellulose-based immunoassays may have blocking agents applied to prevent non-specific binding along the nitrocellulose membrane [5]. Common blocking agents include gelatin, casein, BSA, IgG, PVP, and PVA [5]. There are commercially available tests where the membrane is not actively blocked because the samples contain enough excess protein or the sample pad is supplemented with a blocking agent that prevents non-specific binding [5].

It is difficult to design a LFA for diagnosing a disease with similar symptoms to other diseases or to diagnose an individual with multiple co-infections because more than one analyte must be identified for correct diagnosis [37]. This explains the need to develop multiplexed LFAs that can detect multiple biomarkers. For example, work conducted by Zhao et al. showed a feasible design of a 10-channel lateral flow assay that uses up-converting phosphor technology to detect and quantify 10 different foodborne pathogens [38]. Multiplex lateral flow assays are limited by potential cross-reactivity of antibodies, physical space available on typical lateral flow assays, difficulties in multiplex assay manufacturing and quality control [37]. Though research groups have developed multiplex lateral flow assays, few have been translated to a market product.

Lastly, manufacturing precision and cost also contributes to difficulties in producing LFAs. Nitrocellulose membranes can be easily damaged by processing equipment and, for consistency, require machinery capable of achieving very small tolerance [5]. In the production of LFAs, one of the most time consuming steps is strip assembly, which is often done manually [7]. This involves aligning the overlapping components of the assay (sample pad, conjugate pad, membrane and absorbent pad) and adhering them onto a backing card [7]. This process is estimated to occur at a rate of 3-4 assemblies/min/operator [7].

## **1.8 Alternative 3D Printed Porous Media**

Additive manufacturing, otherwise known as 3D printing, is gaining popularity in many manufacturing fields, initially in the automotive and aerospace sectors but now expanding, due to the ability to produce complex geometries [39], [40]. This type of

manufacturing is characterized by direct production from computer generated models [41]. It can be further described as direct or indirect, whereby direct additive manufacturing involves no post-processing and indirect does, for example, require some form of curing, de-binding or sintering [41]. 3D printing has also gained traction in the production of porous media, specifically in the fields of tissue scaffold design, microelectronics and to a lesser extent, membranes for water treatment and other separation processes. The criteria for lateral flow assay materials outlined in Section 1.3 are not all relevant to these applications, however, there is overlap in manufacturability criteria; 3D printing technologies must have the resolution to produce desired pore geometries. Furthermore, there have been a few attempts to directly use 3D printing techniques for lateral flow devices.

There are several categories of 3D printing that have been used in the production of porous media: (1) Material Extrusion (ex. fused deposition molding), (2) Vat Polymerization (ex. stereolithography, digital light processing), (3) Powder Bed Fusion (ex. selective laser sintering, binder jetting), and (4) Laminated Object Manufacturing (ex. selective deposition lamination) [42]. There is potential to modify these technologies for printing lateral flow assay media, especially since only small areas of media are needed per lateral flow device. The primary challenge in transitioning technologies developed for these applications to lateral flow assays is the difference in pore size distribution, porosity requirements and chemical properties. These properties directly correspond to changes in capillary flow rate through the assay, an important metric in the evaluation of lateral flow assays, and to the ability of binding proteins to the surface. There are many reviews of 3D

printing technologies in the field of wastewater membranes that outline the key print specifications, including resolution, and the advantages and disadvantages associated with each technology [39], [41], [42]. So far in the field, only two-photon polymerization, some forms of stereolithography, and printing using inks containing sacrificial templates are able to achieve resolutions in the nanometer range, with most other technologies having resolutions over 100  $\mu\text{m}$  [42]–[44]. Table 2 summarizes examples of 3D printing of porous media research.

Even with resolution capabilities and accuracy allowing for pore sizes that rival porous media formulated through traditional means like phase inversion, there is currently little incentive to invest in 3D printing for most applications. This is primarily because the smaller the resolution of the print and the greater the print area, which can be up to 10 m by 5 m for a flat-sheet membrane, the greater the print times [45]. Material choice is also still limited.

Table 3. Examples of research into 3D Printing of Porous Media

Application Type	3D Printing Category	Material	Printing Technology	Specific Application	Pore Size Range	Key Observations	Limitations	Ref.
Tissue Scaffold	Material Extrusion	Cellulose Acetate	3D Bioplotter	Osteoblast adhesion/proliferation	99-608 $\mu\text{m}$	Needed a solvent to assist in printing. Four parameters for print optimization: printing pressure, speed, needle offset, ink composition.	After each layer, 5-10 s of drying was needed. Nozzle clogging frequently occurred.	[46]
Tissue Scaffold	Powder Bed Fusion	Calcium Sulfate	Powder-Based 3D Zprinter 450 Printer	Bone regeneration	0.4-0.8 mm	The process described is indirect additive manufacturing, where de-powdering is required after drying. Key parameters were layer thickness, time between layer addition, and print orientation.	Pore size of 0.4 mm had non-removable powder. Pore sizes of 0.4-0.8 had geometric defects. Deviation from CAD design of up to 0.6 mm.	[47]
Tissue Scaffold	Material Extrusion	PEEK	Aon3D FDM Printer	Pre-osteoblast proliferation	800-1800 $\mu\text{m}$	PEEK was treated with sodium hydroxide to improve hydrophilicity.	Nozzle and base plate temperatures must be kept at 390°C and 110°C, respectively.	[48]
Membranes for Water Treatment	Stereolithography	Alumina Powder	Not specified or made-in-house	Ultrafiltration	7.9-13.7 nm	Using smaller sized alumina resulted in smaller pore sizes and using a combination of small and large particles resulted in larger pore size.	The slurry used must be homogeneous, therefore, aggregation must be prevented. Alumina particles are irregularly shaped which can influence pore area.	[44]
General	Direct Ink Writing with Sacrificial Templates (Material Extrusion)	Silica and silica-alumina	3D Discovery	Not specified	10-100 $\mu\text{m}$ 150-1000 nm	Pore size is tunable. Have the option of printing a nano or microemulsion or combining them (two level hierarchical porosity).	Requires drying and sintering. No detail about rheological limitations of printer or mechanical properties of print.	[43]
General	Material Extrusion	Pectin with carboxylated-cellulose nanofibrils	3D Discovery	Not specified	~1 mm	Width of print can be controlled with ratio of nanocellulose and pectin and feed rate of extrusion.	Focus application seems to be general bio-scaffolding. No indication of potential in other applications.	[49]
Synthetic Microfluidic Paper	Multi-directional UV-lithography	Off-stoichiometry thiol-ene	Not specified or made in house	Capillary flow device	Not specified	UV grafting of HEMA hydrophilized the surface. Liquid front velocities of 2.0 mm/s <sup>1/2</sup> were measured.	Cannot completely prevent pillar collapse.	[50]

## **1.9 Printable Calcium Carbonate as an Alternative Material to Nitrocellulose**

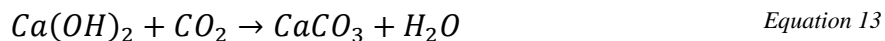
In 2015, a group from Aalto University first reported the use of modified calcium carbonate (MCC)-based coatings for liquid wicking, wherein they compared it to fumed silica, natural diatomite, and flux-calcined diatomite [51]. The binders investigated in the study include styrene-acrylate latex, fully hydrolyzed polyvinyl alcohol, and carboxymethyl cellulose (CMC). Sodium polyacrylate and CMC were further investigated as dispersants. It was found that faster adsorption resulted from incorporating larger pigment particles like diatomite with MCC (high porosity, loose packing) and that, of the binders tested, latex resulted in the highest wicking distance. This work was followed by further work from the same group that investigated using inkjet-printed polystyrene and alkyl ketene dimer hydrophobic patterning of calcium carbonate coated cellulosic paper to create array channels [52]. Biological lateral flow assay applications were explored next where they developed a cytochrome P450 detection system that can be manufactured at a lower cost than assays currently available [53]. Finally, the group investigated the use of coatings with a bimodal pore structure that allows for both control of bulk flow and capillarity. This study looked at different coating formulations, with micro-fibrillated cellulose being the binder of choice, and the benefit of altering coating charge through inkjet printing of polyelectrolytes on the coatings as compared to adding polyelectrolytes to the coating ink formulation [54].

## 1.10 Material Properties of Calcium Carbonate

Calcium carbonate ( $\text{CaCO}_3$ ) is a widely used industrial chemical in the fields of paper, pharmaceuticals, and paint manufacturing [55]. It occurs in many forms, three hydrated (calcium carbonate monohydrate, calcium carbonate hexahydrate, amorphous calcium carbonate) and three anhydrous precipitated forms (calcite, aragonite, vaterite) [55], [56]. The formation of one polymorph over another depends on temperature and the degree of saturation and can be determined through powder X-ray diffraction [56], [57]. Calcite is the most thermodynamically stable of the anhydrous precipitated forms [58]. Calcite has a zero point charge between pH 8 to 9.5 and produces  $\text{Ca}^{2+}$ ,  $\text{HCO}_2^-$ ,  $\text{CO}_3^-$ ,  $\text{H}^+$ , and  $\text{OH}^-$  ions upon dissolution in water [59].

Precipitated calcium carbonate (PCC) is a calcium carbonate product derived from lime. It differs from naturally occurring ground calcium carbonate (GCC) in its narrow particle size distribution, regular shape, and purity [60]. There are multiple routes that can be used to manufacture PCC, one commonly mentioned being the solid-liquid-gas route, otherwise known as the carbonation method [60]. This method begins with the calcination of quarried limestone to make calcium oxide [61]. The calcium oxide is then slaked with water, producing calcium hydroxide. When reacted with carbon dioxide, the calcium hydroxide is converted to calcium carbonate. The chemical reactions occurring in this process are shown in Equations 11, 12, and 13.





A second method of producing PCC, referred to as the liquid-liquid route or calcium chloride process uses carbonate salts instead of  $\text{CO}_2$ , as shown in Equation 14 [60].



There has been substantial research conducted to determine how the calcium carbonate can be modified for specific applications. Functionalized calcium carbonate (FCC), otherwise known as modified calcium carbonate (MCC), can be made by treating calcium carbonate particles with acid which produces  $\text{CO}_2$  that reforms the newly functionalized calcium carbonate structure [62]. When phosphoric acid is used in this process, it produces hydroxyapatite-containing calcium carbonate particles [62]. MCC is industrially manufactured and sold by Omya Inc. as a matting agent for paint and is advertised as having an optimal and controlled shape and surface structure [63].

## 1.11 Objectives

In 2019, researchers from McMaster University continued the investigation of calcium carbonate-based lateral flow assay media [64]. It was found that a dispersion of calcium carbonate in a latex binder can be ejected onto a glass surface and produce a coating. This ejection was done through a pre-programmed non-contact lateral flow dispenser. The wicking rate across the coating was manipulated by making dispersions with calcium carbonate particles of different sizes. It was further shown that some enzymes, specifically alkaline phosphatase (ALP), strongly adsorb to calcium carbonate particles and can retain activity after binding. This was functionally demonstrated by printing a line of

the ALP-bound calcium carbonate-latex dispersion onto a printed lane of non-ALP bound calcium carbonate-latex dispersion. A solution containing 5-bromo-4-chloro-3-indolyl phosphate (BCIP)/ nitro blue tetrazolium (NBT) was wicked through the calcium carbonate lane, producing a purple precipitate when the reaction between BCIP/NBT was catalyzed by the ALP that was bound to calcium carbonate. The purple precipitate was concentrated on the line where the ALP-bound calcium carbonate-latex dispersion was deposited.

As previously discussed, non-specific protein binding causes issues in biological assays, as it can decrease test sensitivity. The work conducted by Alto University and McMaster University researchers has provided evidence of the utility of calcium carbonate as a possible lateral flow assay media. Different calcium carbonate types and combinations can be used to manipulate the rate of wicking, and protein binding to calcium carbonate readily occurs. However, if protein binding can not be prevented, the utility of calcium carbonate as a lateral flow assay media is severely diminished.

The purpose of the work described in this report was to evaluate the feasibility of replacing nitrocellulose membranes with printable calcium carbonate suspensions as the porous media of LFAs. First the properties of different types of calcium carbonate, the effect of ink formulation and treatment on final wicking ability, and the visual characteristics of calcium carbonate-based prints were examined. Second, prevention of non-specific protein binding to calcium carbonate was investigated by treating calcium carbonate particles with blocking proteins and through PEGylation. Third, the impact of blocking calcium carbonate particles on the wicking flow dynamics was examined by creating a dispersion of the blocked calcium carbonate in binder, printing the solution onto

a support, and conducting wicking rate tests. The results of both investigations assess the viability of blocking non-specific binding in a lateral flow assay using calcium carbonate substrate. Finally, a comprehensive comparison of printable porous media beyond that of calcium carbonate for LFAs was conducted. LFAs are a thoroughly reviewed area of study, with nitrocellulose-based technologies being the most common. Little exists in the realm of printable porous media for LFAs and no reviews have been written. Particularly, emphasis was placed on exploring printing materials and technologies, like 3D printing platforms.

## **2 METHODS**

### **2.1 Evaluation of the Properties of Precipitated Calcium Carbonate**

#### *2.1.1 Experimental Design*

A thorough understanding of the properties of three types of calcium carbonate particles was necessary to know the interaction between the particles in solution, between particles and binding components in printed coatings and between the printed coatings and the printing surface. The specific surface area, size distribution and zeta potential of the calcium carbonate particles were measured and compared. Further information about particle characteristics were observed through microscope images of the particles.

#### *2.1.2 Materials*

ViCALity Light precipitated calcium carbonate, to be further referred to as Light PCC or LPCC, was provided by Specialty Minerals Inc. (Adams MA, USA). Omyamatt 75-ME and Omyamatt 100-ME modified calcium carbonate, to be further referred to as

MCC 75 and MCC 100 respectively, were provided by Omya International (Oftringen, Switzerland).

### *2.1.3 Experimental Methods*

Particle size distribution measurements were obtained using the Mastersizer 2000. Specific surface area (SSA), pore volume, and half-pore width were measured using the Quantachrome Instruments Autosorb iQ automated gas sorption analyzer. The Mastersizer 2000 applies Mie scattering theory in the determination of particle size distribution while the Quantachrome applies BET theory for measurement of surface area and Density-functional theory for pore volume and half-pore width. An Olympus upright BX53 microscope was used to obtain magnified images of calcium carbonate samples.

## **2.2 Ink Formulation Factors Affecting Wicking Rate**

### *2.2.1 Experimental Design*

Prior work conducted by Li et al. determined an optimal ink composition for printing calcium carbonate coatings, composed of 15 wt% light calcium carbonate and 1.12 wt% Acronal S728 in 1 mM NaHCO<sub>3</sub> [64]. This ink formulation and post-printing treatment were varied to determine the effect of the changes on wicking rate.

Firstly, a Design of Experiments (DOE) was conducted to model the effect of different ink factors on wicking rate. Shown in Table 4 is the 3-factor, 2-level DOE conditions investigated. The three factors include: (1) binder concentration, (2) PCC concentration, (3) type of PCC. MCC 100 was not included to keep the DOE to 2 levels.

*Table 4. Conditions for the 3-factor, 2-level DOE investigating ink formulation on wicking rate.*

<b>DOE Level</b>	<b>B Binder Concentration (%)</b>	<b>C PCC Concentration (%)</b>	<b>P Type of PCC</b>
(-)	1.12	15	PCC Light
(+)	5	20	MCC 75

Secondly, the effect of mixing different types of calcium carbonate was investigated. By combining the three calcium carbonate types pairwise, a wicking rate intermediate to both was expected. The results from this trial would enable more ways of controlling the wicking rate of the printed porous media.

Thirdly, beyond modifying the formulation of the ink, post-printing modification can be done to alter print characteristics. Specifically, heating the prints to above the glass transition temperature of the binder was theorized to improve the mechanical durability of the print as the latex polymer in the coating would assume a more flexible, amorphous state [65]. Calcium carbonate coatings made with the original formulation by Li et al. printed on glass slides are brittle and susceptible to scratches. This poses future problems for manufacturing and consumer use. A single formulation of ink was tested to see the difference in print durability and wicking rate with and without heating the prints.

Lastly, microscope images of printed ink were taken to observe the surface features of calcium-carbonate based prints. Of specific interest are areas of non-uniformity, and variations between the edges and bulk of the print. Observable differences between light PCC and modified calcium carbonate were noted.

### 2.2.2 *Materials*

Light PCC, MCC 75 and MCC 100 were supplied as previously mentioned in Section 2.1.2. Acronal S728 styrene/n-butyl acrylate copolymer (50 wt% solids) was provided by BASF (Mississauga, Canada). Sodium bicarbonate ( $\text{NaHCO}_3$ ) was purchased from Caledon Laboratory Chemicals (Georgetown, Canada). Ethanol from Commercial Alcohols by Greenfield Global (Brampton ON, Canada) was available on-hand in the McMaster Biointerfaces facility.

### 2.2.3 *Experimental Methods*

Glass slides onto which coatings were printed were cleaned by immersion in a 70% ethanol solution for at least 12 hours followed by an hour of sonication. With minimal contact, the glass slides were removed from the 70% ethanol solution, rinsed with hot tap water, and given a final rinse with DI water. An air stream was used to remove water from the glass slides prior to suspending them to air dry for at least 3 hours or until visibly dry in a fume hood. The slides were stored in a dust/contaminant free container prior to use.

Calcium carbonate – latex inks were made with 15 wt% calcium carbonate, either Light PCC, MCC 75 or MCC 100, and 1.12 wt% Acronal S728 in 1 mM  $\text{NaHCO}_3$ . Variations to the ink composition were made for the DOE, where weight percent composition follows that outlined in Table 4. The dispersions were left to mix on a plate mixer for 12 hours. For experiments investigating combining calcium carbonate types, final combined inks were composed of 50 wt% of one ink and 50 wt% of another. Immediately before use, the dispersions were vortexed on the highest vortex setting for 10 seconds. A Biodot XYZ3060 Dispenser was used to apply ink to glass slides. The ink was ejected in a

line configuration at a rate of 1  $\mu\text{L}/\text{cm}$ , with a drop volume of 50 nL. Coordinates of the start point, and length of print were selected based on the length restrictions of the glass slide. The Biodot base moved at a speed of 10 mm/s as the ink was ejected. Prints were left to dry for approximately 12 hours. Microscope images of printed ink surface were taken with an Olympus upright BX53 microscope. For heated print trials, the printed samples consisted of light PCC ink and were placed in an oven at 90°C for 5 minutes.

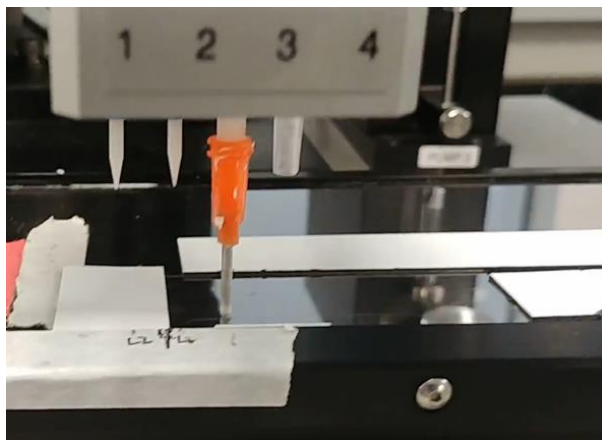


Figure 3. Biodot XYZ3060 Dispenser extruding calcium carbonate ink onto glass microscope slide.

The wicking rate of printed calcium carbonate inks was measured by filling a transparent container with 1 mM  $\text{NaHCO}_3$  to which a printed glass slide is placed vertically. Enough  $\text{NaHCO}_3$  solution was added to ensure about 5 mm of the base of the print was immersed. Video of the wicking through the print was recorded using an LG G6 Smartphone for a total of 10 minutes. Still images from the video were taken every 5 seconds using VLC Media Player. The images were analyzed in ImageJ where the distance travelled by the wetting front from the solution-air interface was measured. Minitab 17 was used for DOE analysis and to produce DOE-specific figures.

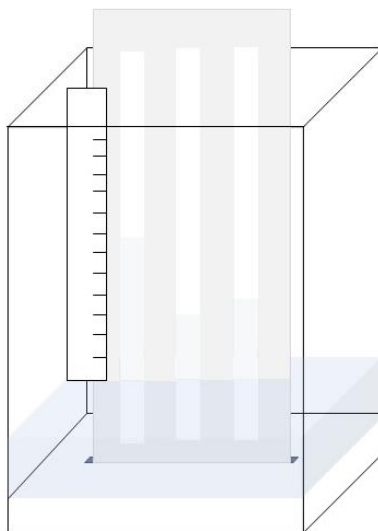


Figure 4. Schematic of a printed glass slide sample set up for a vertical wicking rate test.

## 2.3 Blocking Protein Adsorption to Calcium Carbonate in Solution

### 2.3.1 Experimental Design

The efficacy of surface treating calcium carbonate particles in solution against protein binding was evaluated. The model protein to be blocked from binding was alkaline phosphatase (ALP), which had previously been shown to bind well to calcium carbonate [64]. As a phosphatase enzyme, ALP catalyzes the hydrolysis of phosphate esters [66]. This functionality can be used to quantify ALP activity. Two groups of blockers were considered in the blocking investigation: 1) Protein-based blockers, and 2) Polyethylene glycol derivative blockers.

### 2.3.2 Materials

Alkaline phosphatase (ALP) from bovine intestinal mucosa, p-nitrophenyl phosphate liquid substrate (p-NPP), casein from bovine milk, diethanolamine (>99.5%), magnesium chloride hexahydrate, and sodium hydroxide (50% solution in water) were

purchased from Sigma-Aldrich. Methoxy PEG Phosphate (5000 Da), to be further referred to as PEG-P, was purchased from Jenkem Technology (Plano TX, USA). Bovine Serum Albumin (lyophilized) was purchased from ICN Biomedicals Inc. (Aurora OH, USA) and 10× Liquid Concentrate Phosphate Buffered Saline (PBS) was purchased from BioShop Canada Inc. (Burlington ON, Canada).

### *2.3.3 Experimental Methods*

Protein-based blocking of calcium carbonate was done with BSA and casein proteins. Blocking solutions were prepared by dissolving either BSA or casein in 1×PBS (pH 7.4) to a final concentration of 1 w/v%. Calcium carbonate samples, Light PCC, MCC 75 and MCC 100, were weighed so that the final concentration upon adding the blocking solution was 95.3 mg per 1 mL of solution. Samples were vortexed for 10 seconds on medium intensity and then placed on a plate mixer for 12 hours at room temperature. PEGylation was done similarly where in place of 1×PBS, 1 M diethanolamine (DEA) buffer was used to dissolve the PEG-P to a final concentration of 1 w/v%. Following 12 hours of mixing with blocking solution, the samples were centrifuged for 15 minutes at 4000 rpm. The supernatant was removed, and 1 mL of fresh buffer was added to the remaining calcium carbonate pellet. The pellet was re-dispersed with brief mixing using a vortex. The centrifugation-washing procedure was repeated a total of three times to remove non-bound blocking protein or PEG-P.

Following particle pre-treatment, the calcium carbonate samples were exposed to ALP. A 50 µg/mL solution of ALP in DEA buffer was made and 1 mL was added to each calcium carbonate sample. The samples were vortexed for 10 seconds and then left mixing

on a plate mixer for 12 hours. After mixing, the samples were centrifuged for 15 minutes at 4000 rpm. The supernatant was removed and retained for further analysis.

The amount of active ALP in the supernatant solution was determined by measuring the degree of hydrolysis achieved when added to a p-NPP solution. In a 96-well plate well, 60  $\mu\text{L}$  of p-NPP solution was mixed with 15  $\mu\text{L}$  of supernatant. The well-plate was transferred to a well-plate shaker where it was left to mix at 100 rpm for 5 minutes. The reaction was stopped by adding 125  $\mu\text{L}$  of 3M NaOH. The absorbance of the wells at 405 nm was immediately read.

## **2.4 Wicking Tests with Blocked Calcium Carbonate**

### *2.4.1 Experimental Design*

The wicking rates of coatings containing blocked and unblocked calcium carbonate were compared. Of the blocking mechanisms investigated in Section 2.1, the experiment was only carried out with BSA blocked calcium carbonate. Future work should consider the effect of other blocking methods. As previously mentioned, in the manufacturing of porous media for LFA applications, the wicking rate is a key quality control characteristic. If wicking rate is severely diminished through blocking, alternative blocking methods should be considered.

### *2.4.2 Materials*

The materials used were the same as those outlined in Section 2.2.2 and 2.3.2.

### 2.4.3 Experimental Methods

Blocked calcium carbonate was made as per the protocols in section 2.3.3. It was then incorporated into ink and printed as per the protocols in Section 2.2.3.

## 3 RESULTS AND DISCUSSION

### 3.1 Evaluation of the Properties of Precipitated Calcium Carbonate

Key particle properties of light PCC, MCC 75, and MCC 100 are summarized in Table 5. Light PCC has the smallest particle size of the three calcium carbonate types investigated with the lowest pore volume and specific surface area. MCC 75 and MCC 100 have comparable pore volumes, with MCC 100 having a slightly larger particle size and a correspondingly smaller specific surface area. The zeta potential of the three particle types were also measured, however, the lack of reproducibility in the measurements only concluded that the particles are negatively charged. Figure 5 shows magnified images of Light PCC, MCC 75, and MCC 100. The size distribution of the particles is confirmed with these images. Particle aggregation does seem to occur with all three calcium carbonate types but is most apparent with Light PCC.

*Table 5. Properties of light PCC, MCC 75 and MCC 100. Specific surface area (SSA) was determined using BET method, the pore volume and half-pore width were measured using DFT method and particle size distribution was measured using MIE theory method.*

PCC Type	SSA (m <sup>2</sup> /g)	Pore Volume (cm <sup>3</sup> /g)	Half-Pore Width (Å)	Particle Size Distribution (µm)
Light PCC	10.01	0.03	13.85	d(0.1): 2.867 d(0.5): 7.219 d(0.9): 14.115
MCC 75	55.65	0.35	80.07	d(0.1): 1.698 d(0.5): 17.761 d(0.9): 36.392
MCC 100	45.93	0.34	8.44	d(0.1): 1.916 d(0.5): 21.284 d(0.9): 44.100

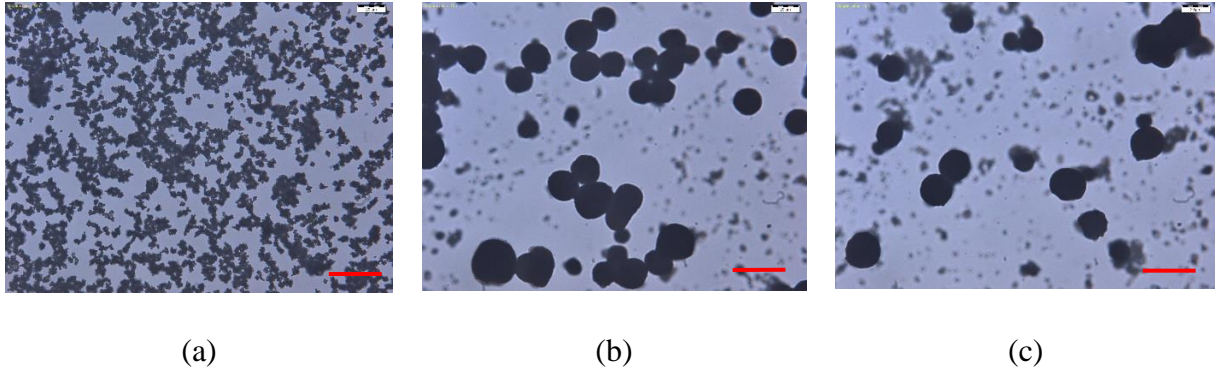


Figure 5. Magnification of (a) LPCC, (b) MCC 75, (c) MCC 100 particles in 1mM NaHCO<sub>3</sub>. A magnification level of 40× was used in all images. Red scale bars indicate 40 μm in the image.

The chemical properties of precipitated calcium carbonate were not explicitly tested in the course of this work. Section 1.10 gave an overview of the structure of calcium carbonate polymorphs and the general chemical process of manufacturing precipitated calcium carbonate. However, understanding the chemical properties is important in assessing how precipitated calcium carbonate reacts in different suspension mixtures and with potential LFA samples. Biological samples typically consist of compounds with phosphate, hydroxyl, amino and methyl groups. These functional groups can interact with calcium carbonate, thus creating undesired dynamic calcium carbonate systems. Of interest is the interaction of phosphates with calcium carbonate, which has been studied for some time. In solutions with low phosphate concentration, phosphate adsorbs onto the calcium carbonate crystal surface and in solutions with high concentrations, dicalcium phosphate forms [67]. Further experiments looking at reaction rates found that phosphate solutions reached equilibrium relatively quickly with solid calcium carbonate but not calcium phosphate [67]. Equilibrium between calcium phosphate and hydroxyapatite is reached much slower [67].

## **3.2 Ink Formulation Factors Affecting Wicking Rate**

### *3.2.1 DOE Investigating the Effect of Ink Composition on Wicking Rate*

The capillary flow rate experimental results from the full factorial DOE investigating three ink formulation factors (binder concentration, B, PCC concentration, C, type of PCC, P) at two levels are summarized in Table 6. Table 7 shows the outcome of the DOE and the p-value for each term. Terms with p-values less than  $\alpha = 0.05$  are deemed significant to the model. Equation 15 is the resulting model relating wicking rate to the factors tested omitting insignificant terms. The effects of each of the factors on the wicking rate are further visualized in the Pareto plot shown in Figure 6 where bars that extend beyond the red reference line are significant. The Pareto plot indicates that in terms of standardized effect, binder concentration has the greatest effect on wicking rate, followed by the type of calcium carbonate used. Contrastingly, the concentration of calcium carbonate has a relatively insignificant effect. This may provide an opportunity to decrease the viscosity of the ink solution by decreasing calcium carbonate concentration without significantly compromising wicking rate of the print. Improved modeling results could be obtained by testing larger level ranges. Specifically, the two levels of calcium carbonate concentrations used would ideally cover a larger concentration range.

Table 6. DOE summary and results for the investigation of ink composition on wicking rate. The factors investigated include binder concentration, B, PCC concentration, C, type of PCC, P. Actual run refers to the order in which the experiment was performed and the Design Run refers to the order in which the experiment was designed.

Actual Run	Design Run	B	C	P	Average Wicking Rate (mm/s <sup>1/2</sup> )
3	1	-	-	-	1.93
6	2	+	-	-	1.36
5	3	-	+	-	1.41
7	4	+	+	-	1.22
1	5	-	-	+	1.35
8	6	+	-	+	0.39
2	7	-	+	+	1.40
4	8	+	+	+	0.49

Table 7. DOE model coefficients and P-values for analysis of term significance.

Term	Uncoded Coefficient	Coded Coefficient	P-Value	P-Value <0.05
B	- 0.0364	-0.03293	0.000	Yes
C	- 0.0059	-0.00633	0.093	No
P	- 0.1251	-0.02865	0.000	Yes
BC	0.0011	0.00538	0.148	No
BP	0.0080	-0.01413	0.001	Yes
CP	0.0068	0.01029	0.010	Yes
BCP	- 0.0008	-0.00423	0.250	No
Constant	0.2751	0.11938	0.000	Yes

$$\text{Wicking Rate} = 0.2751 - 0.0364B - 0.1251P + 0.0080BP + 0.0068CP$$

Equation 15

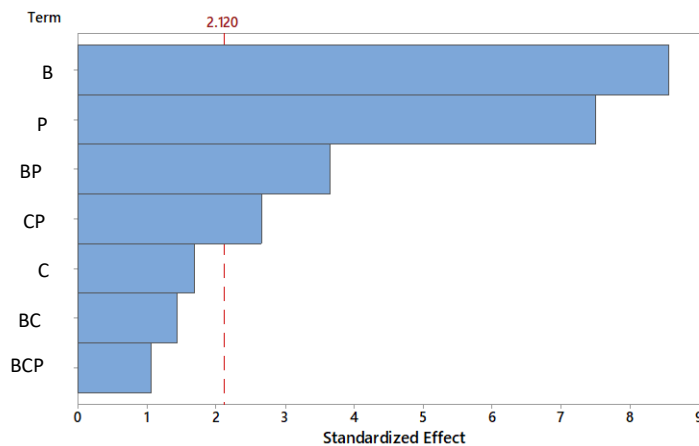


Figure 6. Pareto plot showing the absolute value of the effects of binder concentration, B, calcium carbonate type, P, and calcium carbonate concentration, C. Interaction of the effects is also shown. An  $\alpha$  value of 0.05 was used in the analysis.

Most of the two and three factor interaction effects have relatively little influence on wicking rate. Of the multiple factor interactions, the interaction of binder concentration and calcium carbonate type had a relatively large influence on wicking rate. This may be attributed to the difference in pore volume of the different calcium carbonate types. MCC 75 has a pore volume ten times greater than that of light PCC, therefore, increasing binder concentration can block the pore network of light PCC more completely as compared to MCC 75.

The results of the wicking rate DOE bring into the forefront questions about the interaction of calcium carbonate with the latex binder in the coating. Specifically, the void network formed by calcium carbonate and latex in the coating dictates flow through the medium. There are two types of porous spaces in the coatings: (1) the interparticle space, and (2) the intraparticle pores [54]. Work by Jutila et al. demonstrated that bulk flow is dictated by interparticle space by acting as reservoirs, while intraparticle pores primarily enable capillarity and the binding of reactants [54]. The fluid dynamic modelling of flow through bimodal porous networks is well-described by researchers from Omya AG who published several reports on the topic in the early 2000s [68]–[70]. In these modelling studies however, no binders were used, instead the calcium carbonate was pressed into tablets. The addition of binders is known to block both inter- and intra- particle spaces. Of the two binders examined by Jutila et al., styrene acrylic latex blocked pores to a lesser degree than microfibrillated cellulose, however, the hydrophilicity and hygroscopic nature of microfibrillated cellulose allowed for faster wicking [54]. Interestingly, in preliminary binder trials in this work, binders with high hydrophilicity, like poly (vinyl alcohol), were

found to result in undesired print dissolution upon contact with aqueous wicking solution. Therefore, wicking rate is not the only consideration when substituting a latex binder for one that is cellulose based.

Without the addition of binder and with the assumption that the calcium carbonate particles resemble spheres, models of porous spaces in random packing of spheres can be used to predict the inter-particle porosity achievable with a calcium carbonate-based coating. Numerous studies in the 80s and 90s focused on simulating the random packing of spheres. One study found packing densities of 0.509 to 0.638 for random close packing of spheres of the same size [71]. This corresponds to porosities of 0.401 to 0.378 as compared to 0.69 to 0.77 achievable with nitrocellulose, as stated in Section 1.6. This theoretical limitation in the amount of pore space available in randomly packed spheres detracts from using suspensions of particles for porous materials in place of nitrocellulose.

Beyond theoretical random packing of spheres, research by Gane et. al. looked into modelling and simulating the void space of paper coatings by considering the compressibility of mineral and synthetic pigments and latex binders with spaces that are not intrudable by mercury porosimetry [72]. Of the calcium carbonate types explored in the study, simulations showed that calcium carbonate characterized by a steep size distribution with fewer fine particles had the largest porosity, maximum pore throat size, connectivity between pores and liquid and air permeability [72]. This emphasizes the dependence of interparticle voids on the specific characteristics of the calcium carbonate type. When any of the three latex binders in the study were added to the calcium carbonate, the porosity

decreased by 14% to 26%, which was simulated accurately with the group's modelling [72]. This again validates the observations of the DOE performed. Researchers working with Johnson and Johnson have examined the packing properties of calcium carbonate in PHEMA-co-PMAA hydrogel films [73]. The calcium carbonate used in this study were of aragonite crystal structure, which has a needle-like morphology. The greater the aspect ratio, AR, of the particles ( $AR > 1$ ), i.e. the more elongated, the lower the maximum packing fraction of the particles [73]. Spherical densely packed particles ( $AR = 1$ ) in aqueous suspensions have maximum packing fractions of 0.58 to 0.71 with more irregular but still monodispersed particles having maximum packing fractions of 0.38 to 0.58 [73]. Solutions with higher initial viscosity than a simple aqueous solution would have an even lower packing fraction.

### 3.2.2 *Effect of Heating Print on Wicking Rate*

The wicking rate results of heat-treated printed samples compared to non-heated are shown in Figure 7. The average wicking rate decreased from  $1.88 \text{ mm/s}^{1/2}$  to  $1.17 \text{ mm/s}^{1/2}$  when comparing the non-heated to the heated sample. Two temperature-related properties of polymers must be considered in determining the impact of heating the calcium carbonate-latex prints: (1) Glass transition temperature,  $T_g$ , and (2) Minimum film formation temperature, MFFT. Though these properties are related, MFFT is typically a few degrees lower than  $T_g$  [74]. There are several stages in the process of drying a latex film. Firstly, the aqueous solvent evaporates causing the latex particles to first come into contact and form capillaries [75]. This is followed by complete particle convergence, whereby the capillaries disappear and, finally, deformation, where the particles assemble

into a hexagonal structure [75]. It is during the deformation stage of film formation that the MFFT is of importance. The MFFT is the lowest temperature at which the deformation will occur and particles will coalesce to form a film [76]. By this principle, the results observed in the heated and non-heated coating experiment were expected. Raising the temperature of the binder above the MFFT and  $T_g$  of 23°C results in greater latex mobility and block the interparticle and intraparticle pore spaces [77].

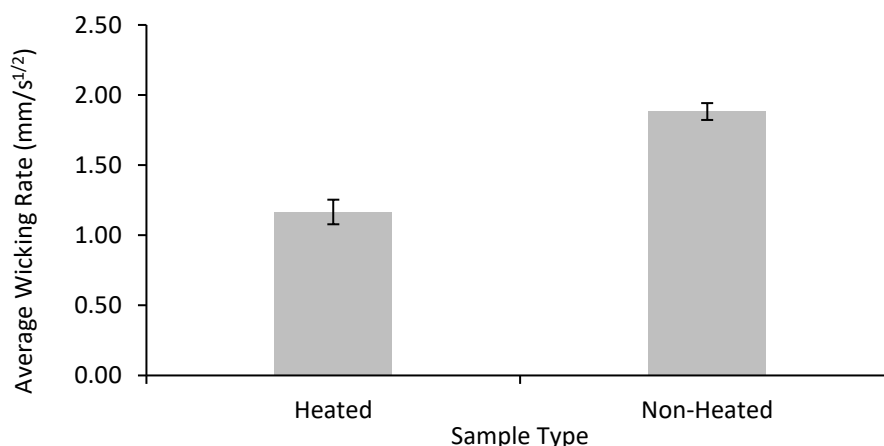


Figure 7 Difference between wicking rates of printed ink heated at 90°C for 5 minutes compared to non-heated. Prints were composed of light PCC.

Although a decrease in wicking rate upon heat treatment is not ideal, it is necessary to prevent temperature dependent coating dynamics. The optimal temperature of lateral flow assays depends on the type of assay being conducted. For example, the ideal temperature for DNA detection was found to be between 55-60°C to promote nucleic acid hybridization, and for antibody-antigen interaction the ideal temperature was found to be between 37-40°C [78]. For this reason, you cannot have components in the porous media that changes flow performance with temperature. This can easily be improved by investigating binders with lower glass transition temperature such that the binder forms a

coalesced film at all working temperatures, heat treating the samples and accounting for the change in wicking rate, or designing an assay that does not incorporate temperature sensitive materials.

### 3.2.3 Effect of Combining Calcium Carbonate Types on Wicking Rate

As previously covered in Section 2.1, three types of calcium carbonate particles with distinct particle properties were compared throughout this report. In addition to having distinct particle properties, when incorporated into an ink, the three calcium carbonate types result in different wicking rates. Figure 8 shows the wicking results of prints made with each of the three calcium carbonate types and with 50 wt% mixes of two of the three types.

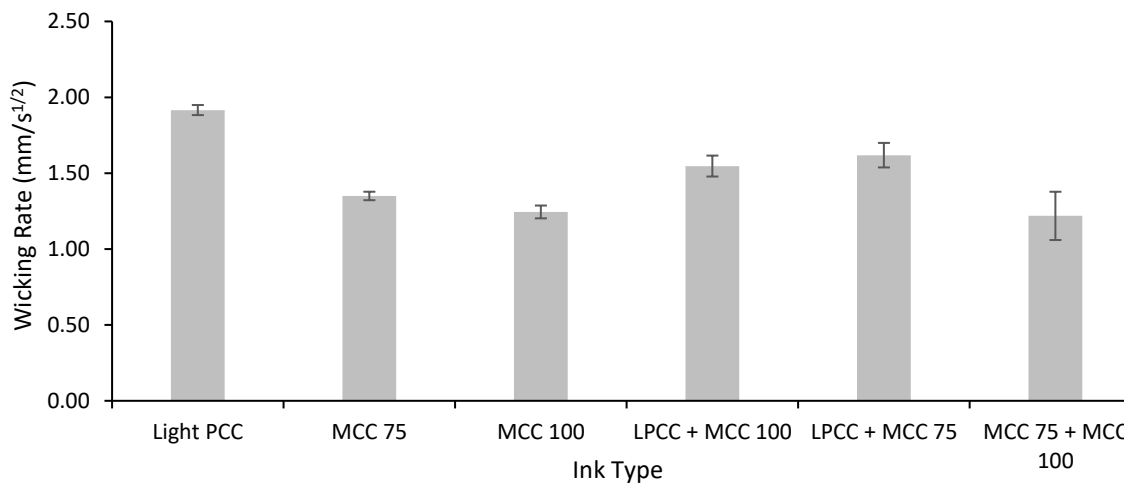


Figure 8. Wicking rates of inks consisting of mixes of calcium carbonate types in comparison to inks of only one calcium carbonate type.

Light PCC had the fastest wicking rate in this set of experiments, with MCC 75 coming second. Furthermore, when light PCC is mixed with either MCC 75 or 100, a wicking rate intermediate to the wicking rates of the individual light PCC and MCC 75 or 100 inks was obtained. This is also observed for the mix of MCC 75 with MCC 100 inks. These results suggest that mixing of particle types may be an effective means of controlling

wicking rate, but further investigations using different mixture proportions would have to be completed to see if desired set wicking rates can be achieved. One study in particular involved the mixing of pigments into a pellet form and investigating the effect on the absorptive capacity [70]. Standard ground calcium carbonate (GCC) and an egg shaped specialty pigment (no further information provided), were used [70]. With increasing proportions of GCC added to the tablet, which has 27% lower porosity than the specialty “egg” pigment, the total porosity of the tablet, the fluid uptake volume and the fluid uptake rate all decreased [70]. The fluid uptake rate observation at 50% ratios was explained by the pore size of the pigments, with the “egg” pigment having a larger number of fine pores, which enable capillary action, and the GCC having fewer fine pores [70]. If applied to the mixing results obtained, without doing any pore size distribution measurements, one might conclude that light PCC has more fine pores that enable capillary movement than either MCC 75 or 100. As discussed in Section 3.1, light PCC actually has a lower pore volume than MCC 75 and 100, which may be due to smaller pore size, or lower porosity. A more thorough investigation of pore structure for all three calcium carbonate types must be performed to understand the impact of mixing calcium carbonate types on flow dynamics in the coatings.

#### *3.2.4 Image Analysis of Printed Ink*

Obtaining defect-free porous material is one of the key challenges in manufacturing nitrocellulose, as described in Section 1.7, so as to ensure reproducible wicking. As a prospective alternative to nitrocellulose, the ability to produce a uniform coating of porous calcium-carbonate ink is therefore important. Confocal microscope images of three areas

of a typical printed ink sample are identified in Figure 9. Areas 1 and 3 focus on the edge of prints while area 2 focuses on the center. Figure 10 shows the magnified images for these target areas for a print consisting of light PCC and MCC 75.

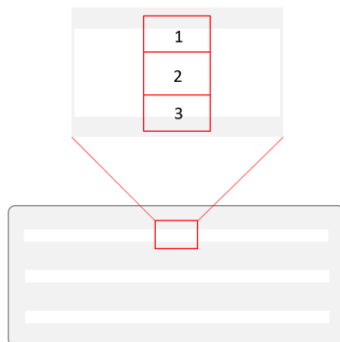


*Figure 9. Imaging areas of a printed ink sample with respect to its location on the microscope slide. A typical print sample has three lanes printed, with the focus of the microscope images being on one of the three. Area 1 shows one edge of the print, area 2 shows the center, and area 3 shows the opposite edge.*

Images of the print edges of both light PCC and MCC 75 show that there is increased non-uniformity and non-covered zones as you move away from the center of the print. This edge-effect is more pronounced in the coating consisting of light PCC. This decreased edge effect is an appreciable advantage for using a modified calcium carbonate over a non-modified precipitated calcium carbonate when producing inks. Additionally, comparing the center of the light PCC print to the MCC 75 print shows dark clusters of particles, suggesting that more mixing may be required than MCC 75 or that they have a stronger tendency to aggregate. Manufacturer data sheets for MCC 75 support these observations, describing MCC 75 as being deliberately and uniquely designed to produce a smooth film surface [79].

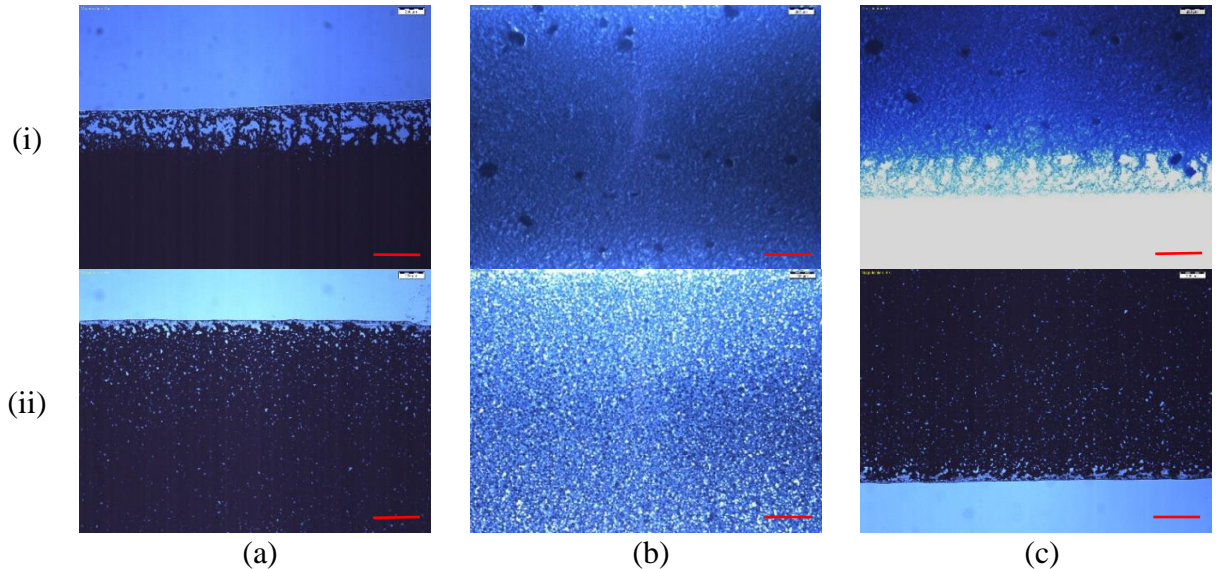


Figure 10. Magnified images of printed ink consisting of (i) 15 wt% LPCC, or (ii) 15 wt% MCC 75, with 1.12 wt% latex binder. Image (a), (b), and (c) correspond to areas 1, 2, 3 indicated in Figure 9. Images taken at 4× magnification level. Red scale bars indicate 400  $\mu\text{m}$  in the image.

Higher magnification images of printed inks composed the three types of calcium carbonate are shown in Figure 11. These images were selected as they clearly show crack-like formations in the coating that could potentially influence wicking flow. These crack-like formations can be attributed to the drying process of the coating when there is stress due to film shrinkage and weak particle-particle adhesion [76]. Typically, if a latex containing film is dried above the MFFT, no cracks should be produced [76]. Apart from experiments specifically looking at the effect of applying heat to coatings, no temperature or humidity control was imposed during film drying. There was also an arbitrary drying time selected which did not necessarily correspond to the time required for complete film formation. This is defined in Section 3.2.2 as the point of coalescence between latex particles. Cracking within the latex coating as seen in Figure 11 may explain non-uniform wetting fronts and other wicking irregularities. If not completely preventable, calcium

carbonate suspensions would not qualify as a superior lateral flow media compared to nitrocellulose.

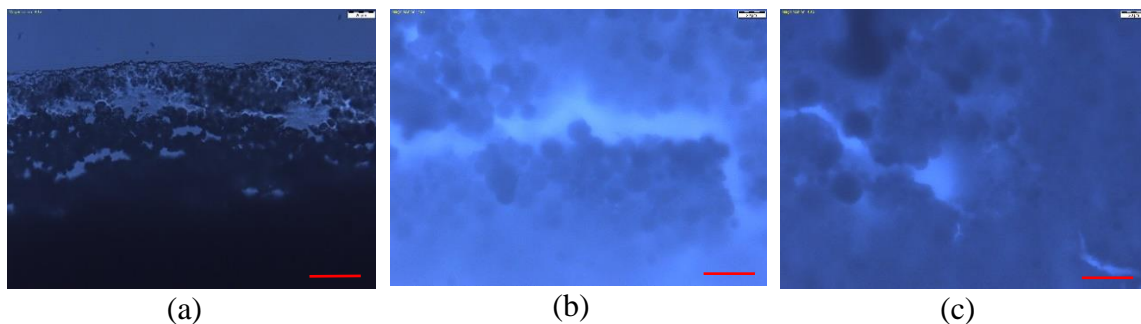


Figure 11. Magnified images of printed (a) 15 wt% LPCC, (b) 15 wt% MCC 75, with 1.12 wt% latex binder. Images were taken at 40 $\times$  magnification level. Red scale bars indicate 40  $\mu$ m in the image.

### 3.3 Blocking Calcium Carbonate in Solution

In blocking porous media, the main goal is to limit undesired protein binding to the media by either sterically or electrostatically blocking access to possible binding sites. As mentioned in Section 1.5, membrane blocking is often achieved using protein pre-treatment, exploiting proteins already present in the sample or using polymer chains.

#### 3.3.1 Casein Blocking

The first investigation of blocking protein binding to calcium carbonate involved pre-treating the three particle types (light PCC, MCC 75 and MCC 100) with casein. Figure 12 shows the results of casein treatment on the fraction of ALP protein adsorbed. Pre-treatment using solvents without casein were used as the control. Two solvents were tested, the first being 1 mM NaHCO<sub>3</sub> and the second being 1 $\times$  PBS, which was also used as the solvent for preparing the casein solutions. The addition of 1 mM NaHCO<sub>3</sub> in the solvent for preparing the casein solutions. The addition of 1 mM NaHCO<sub>3</sub> in the experimental design was intended to investigate whether phosphates in PBS buffer itself interact with the calcium carbonate. The results show a decrease in the fraction of ALP

adsorbed using 1× PBS compared to 1 mM NaHCO<sub>3</sub> even without the addition of casein. Essentially all ALP added to particles pre-treated with only 1 mM NaHCO<sub>3</sub> adsorbed. This is in comparison to the 78%, 90% and 87% adsorbed on light PCC, MCC 75 and MCC 100, respectively, after being pre-treated with only 1× PBS. Pre-treatment using 0.01% and 0.1% casein in 1× PBS showed no significant decrease in the fraction of ALP adsorbed onto any of the three types of calcium carbonate. A more significant reduction in ALP adsorption occurred when the concentration of casein used for blocking was increased to 1%, however, this improved blocking was only evident for MCC 75 and MCC 100.

No higher concentrations of casein were attempted because of the limited improvement observed when increasing the casein concentration from 0.1% to 1%. To confirm that using a higher concentration of casein would be ineffective, a surface saturation coverage estimate of 1 mg/m<sup>2</sup> for polymer adsorption was used to calculate the theoretical minimum amount of casein needed to result in a monolayer on the surface of the calcium carbonate. Based on this estimate of 1 mg/m<sup>2</sup> and the SSAs of the calcium carbonate particles shown in Section 3.1, 0.954 mg, 5.34 mg, and 4.38 mg of casein would be needed to saturate the surface of 95.3 mg of light PCC, MCC 75, and MCC 100, respectively. The amount of casein present in the pre-treatment solution was 10 mg. This makes it unlikely that there was insufficient casein used.

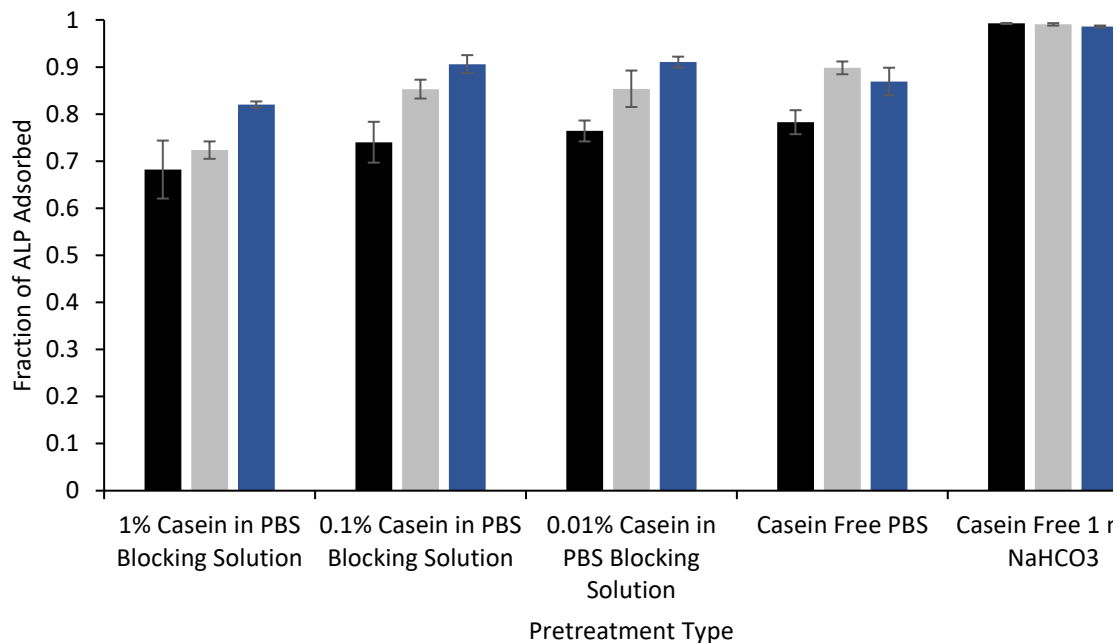


Figure 12. Comparison of adsorbed fraction of ALP on calcium carbonate particles that have and have not undergone casein pre-treatment. Experiments were performed on three calcium carbonate types: LPCC (black), MCC 75 (grey), MCC 100 (blue).

Casein is composed of several phosphorylated polypeptide chains, including  $\alpha_{S1}$  (40 % w/w),  $\alpha_{S2}$  (10 % w/w),  $\beta$  (35 % w/w), and  $\kappa$  (15 % w/w) caseins [80], [81]. These proteins are believed to function as a means of calcium and phosphate transport for bone development in offspring in mammalian milk [80]. Casein proteins are rheomorphic, meaning they have flexible conformations, and they also tend to self associate into micelles in milk [80], [82]. These micelles range from 50 to 600 nm in diameter [83]. The calcium binding ability of casein is made possible due to groups of phosphoserine and phosphothreonine residues [84]. All casein subgroups have a negative charge at neutral pH, with isoelectric points ranging from 4.2 to 5.8 [81], [85]. It is the  $\kappa$ -casein located at the surface of a casein micelle that specifically results in a negative surface charge [83]. The negative surface charge of casein at the pH of the PBS used most likely contributed to the limited ability of the casein to associate with the negatively charged calcium carbonate

particles and block ALP adsorption. The pH of the casein solution should have been, therefore, lowered to imbue a less negative charge on the casein molecules, thereby promoting calcium carbonate blocking. A potential negative consequence of this is particle aggregation. In the dairy industry, milk curd is formed by hydrolyzing  $\kappa$ -casein which decreases negative charge of the casein [83]. Furthermore, PBS is not the ideal solvent to use with ALP as it is known to inhibit phosphatases and interfere in assays using anti-phosphate antibodies [85]. This may have resulted in less ALP binding to calcium carbonate when using 1× PBS as compared to when 1 mM NaHCO<sub>3</sub> was used. Where casein was included in pre-treatment, it is possible that an apparent higher fraction of ALP adsorbed than expected in cases with casein blocking because a portion of the ALP may have been acting on phosphorylated casein residues and not the pNPP hydrolysis reaction. This can potentially explain the limited success of casein blocking and the effect of PBS alone.

Overall, casein pre-treatment as it was conducted did not prevent protein binding to a satisfactory degree. This can be attributed to both unfavorable electrostatic interactions between the calcium carbonate and the casein and potential interference from phosphates in the buffer when conducting the ALP adsorption assay.

### 3.3.2 *BSA Blocking*

The results of pre-treating calcium carbonate with BSA are shown in Figure 13. Only one concentration of BSA was tested based on the monolayer saturation coverage calculation performed in Section 3.3.1. Compared to casein pre-treatment, there was less of a decrease in adsorbed ALP between samples that were not blocked and samples that

were. Therefore, casein affords better blocking than BSA. The use of PBS as a solvent alone impacted the fraction of ALP adsorbed, as was observed in the casein experiments. This observation was previously explained in Section 3.3.1. Only MCC 75 and MCC 100 experienced a notable decrease in adsorbed ALP compared to treatment with PBS without BSA, however this decrease was minimal, at about 9% for both.

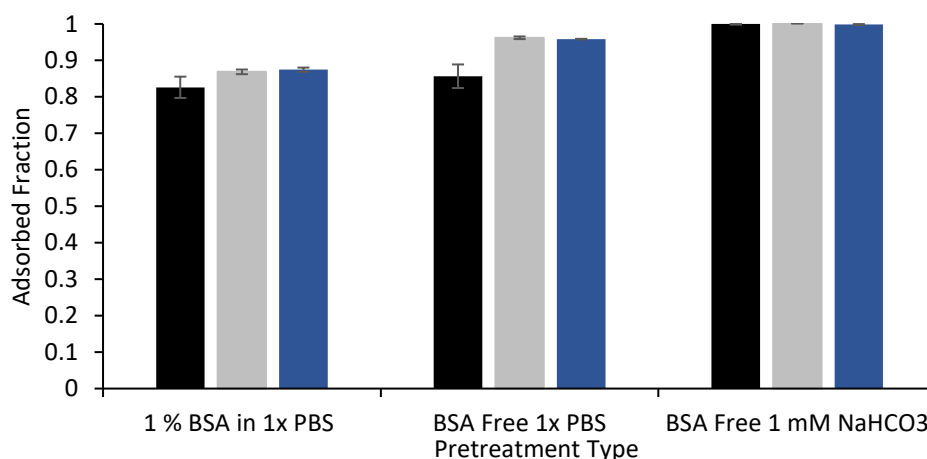


Figure 13. Comparison of adsorbed fraction of ALP on calcium carbonate particles that have and have not undergone BSA pre-treatment. Experiments were performed on three calcium carbonate types: LPCC (black), MCC 75 (grey), MCC 100 (blue).

BSA is a large protein with a molecular weight of 66 kDa and has three binding sites for calcium ions [86]. The isoelectric point of BSA is around 4.7 and 4.8. When the BSA solution pH is above the isoelectric point, the BSA is negatively charged, and the opposite is true when the solution pH is below the isoelectric point [87]. This leads to the same issues experienced with casein, where the pH of the PBS was above the isoelectric point, resulting in negatively charged BSA and unfavourable electrostatic interactions that prevented binding of BSA to calcium carbonate. This was observed in research done by Low et. al., who showed the dependence of pH on BSA binding mechanisms to nitrocellulose [87]. Through this work it was observed that maintaining a pH below the

isoelectric point results in positively charged BSA that binds to negatively charged nitrocellulose [87]. The repulsive forces between the BSA particles below the isoelectric point, however, limits the coverage of the membrane and therefore coverage is actually optimized when the pH is near the isoelectric point [87]. Other studies provide contrasting reports on BSA adsorption, where BSA bound on the following self-assembled monolayers (SAM) in increasing amounts: neutral hydrophilic SAM < neutral hydrophobic SAM < negatively charged SAM = positively charged SAM. Interestingly, BSA bound to negatively and positively charged SAMs in similar amounts [88]. The authors attributed the lack of dependence of surface charge type on the presence of both positive and negative charged residues on BSA [88].

The key difference between these studies and the printing of calcium carbonate are the surfaces onto which the BSA is binding and the difference between two-dimensional and three-dimensional protein interactions. Porous media like nitrocellulose and calcium carbonate-based printed media are not comparable to self-assembled monolayers because of the three-dimensional porous material network that may force close spatial interactions between BSA molecules. This results in greater steric and electrostatic repulsion between BSA molecules, limiting the binding density. This also means that pH, and specifically the dependence of BSA charge on pH, may strongly control the ability to block calcium carbonate porous media.

### 3.3.3 *Phosphorylated PEG Blocking*

Phosphorylated PEG was selected as the final blocking substance for calcium carbonate. The results of the blocking are shown in Figure 14. Only one concentration of

PEG-P was used. No evidence of blocking was observed, with almost 100% of ALP adsorbing on all three types of calcium carbonate pre-treated with PEG-P and not pre-treated.

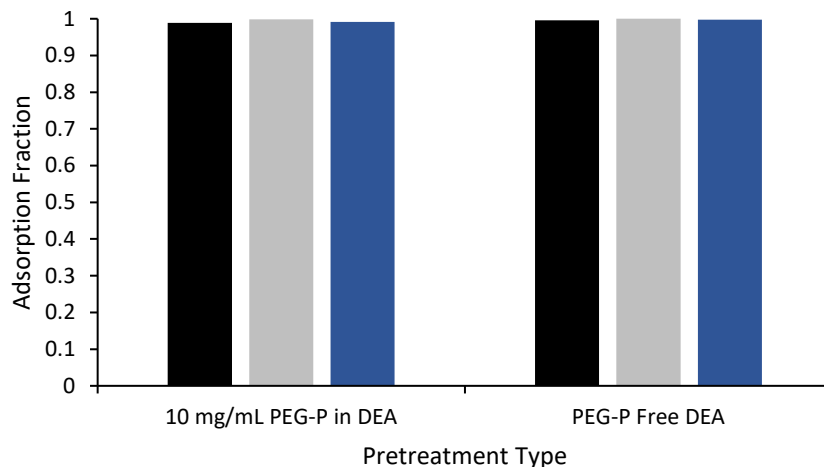


Figure 14. Comparison of adsorbed fraction of ALP on calcium carbonate particles that have and have not undergone PEG-P pre-treatment. Experiments were performed on three calcium carbonate types: LPCC (black), MCC 75 (grey), MCC 100 (blue).

In this experiment, PEG-P was dissolved in DEA buffer instead of PBS to eliminate the possibility of PBS influencing the ALP reaction, as was observed in both casein and BSA blocking. Using DEA for blocking also helped in terms of solvent consistency, as ALP must be solubilized in DEA prior to being added to the blocked or unblocked particles.

There are known interactions between calcium carbonate and orthophosphates that would suggest PEG-P, which has a phosphate group at one end as shown in Figure 15, has effective blocking potential. Orthophosphates form surface complexes with  $\text{CaCO}_3$ , the most thermodynamically stable product of this complexation being hydroxyapatite [67], [89]. This complex formation process occurs in 2 stages: (1) initial rapid surface adsorption of phosphate, and (2) slow precipitation of calcium phosphate [90]. Phosphate will be

released from the surface if the second stage does not occur. The key factors determining extent of calcium phosphate precipitation are phosphate concentration, reaction time, and pH [90]. Work by Li et. al. carried out investigations of how these factors influence phosphate precipitation over a 30-hour period. At pH 7.7, precipitation occurred after 24, 10, 6, and 3 hours for phosphate concentrations of 3, 5, 7.5 and 10 mg/L, respectively [90]. Below these concentrations, no precipitation was observed. At pH 8.3, only with phosphate concentrations of 10 mg/L did precipitation occur in the 30 hour observation window [90]. At even higher pH values, precipitation was not observed. This highlights the main issue when working with DAE as a solvent, which has a pH of 9.8.

The methoxy PEG chain of PEG-P is one of many PEG polymers commonly used to prevent protein binding and to sterically stabilize suspensions [91], [92]. The goal in protein blocking specifically is that the PEG-P molecules create a “brush” over the surface preventing binding.

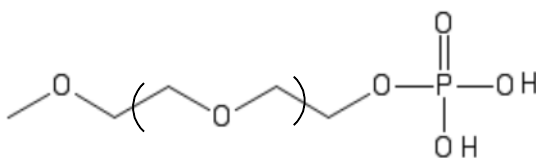


Figure 15. Chemical structure of methoxy PEG phosphate. Recreated using PubChem Sketcher V2.4 from [93].

In a study investigating the binding regimes of different functionalized PEG molecules to calcium carbonate, long chain di-phosphonate functionalized polymer bound most effectively due to the high adsorption free energy [91]. This study showed that the radius of gyration of PEG can be accurately approximated using Equation 16 and applied to determine the saturation coverage at the transition from “mushroom” to “brush”

coverage [91]. With a molecular weight of 5000 Da, the radius of gyration of the PEG-P used is predicted to be 3.1 nm, with a saturation coverage of 0.28 mg/m<sup>2</sup>. For the mass of calcium carbonate used in the experiment and the specific surface area of each type of PCC it was confirmed that based on the findings of this study, the amount of PEG added should have been enough to saturate the surface to reach the “mushroom” to “brush” coverage. It is interesting to address that this study, in contrast to that by Li et. al., claimed that surface adsorption was not dependent on pH, though pH was only adjusted to 11 after an unspecified equilibration time.

$$R_g = 0.0215M_w^{0.583} \text{ nm} \quad \text{Equation 16}$$

### **3.4 Wicking Rate of Coatings Composed of Blocked Calcium Carbonate**

Out of the three blocking trials, none were successful in decreasing protein binding beyond 15%. This can likely be improved by optimizing factors like pH, adsorption/reaction time, and blocker concentration. Even with limited blocking success, it was important to investigate how treating calcium carbonate particles with blocking solutions changes flow through printed calcium carbonate media. Three BSA concentrations were used to pre-treat light PCC calcium carbonate particles. Figure 16 shows the results of wicking distance over time.

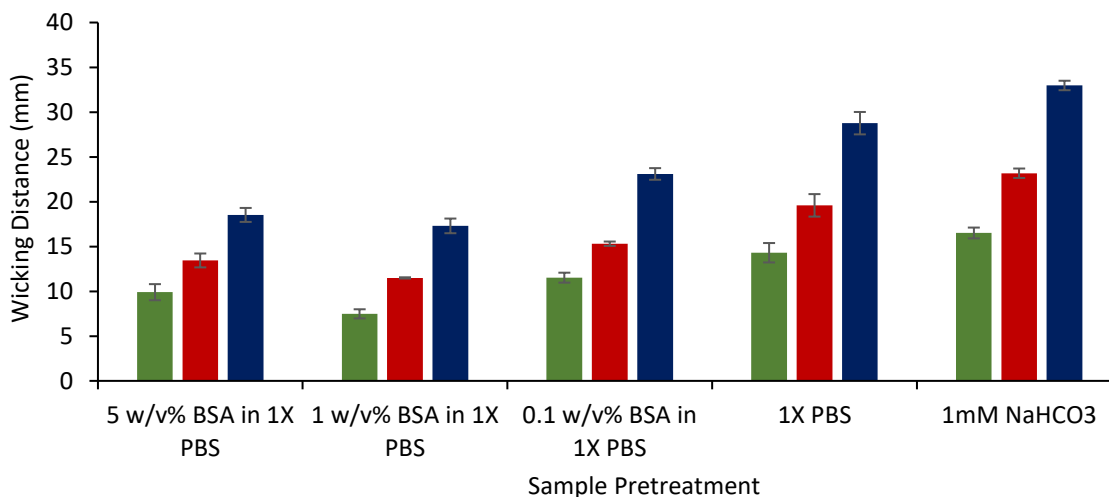


Figure 16. Wicking distance at 1 minute (green), 2 minutes (red), 5 minutes (blue) in prints containing calcium carbonate pre-treated with BSA compared to non-pre-treated calcium carbonate.

Calcium carbonate treated with only PBS has a slower wicking rate than that treated with only 1 mM NaHCO<sub>3</sub>. This suggests that the lower fraction of adsorbed protein observed in Section 3.3.1 and 3.3.2 for samples treated with protein-free PBS compared to protein-free 1 mM NaHCO<sub>3</sub> may be related to a decrease in intra- or interparticle space, which is a common factor influencing both protein binding and wicking rate. The addition of 0.1 w/v % and 1 w/v % BSA resulted in a 20% and 40% reduction in the distance travelled in 5 minutes, respectively, compared to 1× PBS without BSA. This is an important consideration as typical samples used in lateral assays are composed of many proteins which can block pores in the calcium carbonate.

## 4 CONCLUSION

### 4.1 Summary of Results

It was demonstrated that calcium carbonate-based inks can be printed into coatings that facilitate lateral flow. The capillary flow rate can be controlled by varying the type of calcium carbonate used and the concentration of latex added to the ink. The drying

temperature and humidity must be controlled to prevent variations in print structure and subsequent flow patterns. In preventing non-specific protein binding, of the three methods investigated, treating particles with casein was most effective at reducing protein adsorption. The degree of reduction was not enough to conclude casein particle treatment is the optimal blocking method and not enough for application in protein-based immunoassays. There is reason to believe that phosphorylated PEG would be a superior blocker if the binding of the phosphate functional end group to calcium carbonate was optimized. This includes varying adsorption time, pH, and temperature, according to literature findings. The method of applying the blocking solution can also be varied. The application process used in this work involved pre-treating calcium carbonate particles prior to formulating inks for printing. However, it may be more effective to print the coatings using unblocked particles and then immerse the print in blocking solution, as is done with nitrocellulose. Another alternative would involve inkjet application of blocking solution onto an unblocked printed coating which would enable selection of where it is to be applied. Blocking non-specific binding, though necessary to increase assay sensitivity, decreases the capillary wicking rate through the calcium carbonate porous media. The decrease that occurs must be considered when choosing other factors that effect the capillary flow rate, such as ink composition. In this way, the porous media can have both the desired flow rate and limited non-specific protein binding.

## **4.2 Comparing Calcium Carbonate Based Media to Other 3D Printing Forms**

Printed PCC media must be directly compared to other alternative porous medias to conclude whether it is worth pursuing in lateral flow assay development. The metrics outlined in Section 1.3 will be used as the point of comparison. Table 8 shows a weighted Pugh matrix comparing PCC, two examples of 3D-printed porous media and filter paper. Nitrocellulose is the baseline porous media currently used in many lateral flow assay applications. As such, in the table, nitrocellulose is assigned values of 0 for metrics. In a weighted Pugh matrix, each metric is given a weight from 1 to 5 based on the relative importance of the metric. For each alternative porous media, a value of -1, 0, or +1 is assigned if the alternative performs worse than the baseline in a metric, equivalent to the baseline, or better than the baseline, respectively. This comparison is qualitative, and some metrics were not explicitly studied, in which case a score of 0 was assigned, meaning it was assumed to be equivalent to nitrocellulose. Furthermore, some of the metrics are highly dependent on the type of assay being performed and were not considered. As such, with more research and investigation, the conclusions from this comparison may change.

Table 8. Weighted Pugh matrix comparing porous membranes: NC (nitrocellulose), C (cellulose/paper [13]), PCC (precipitated calcium carbonate), 3D-1 (Material extrusion of ink composed of sacrificial templates with silica (refer to Table 3)), 3D-2 (Multi-directional UV lithography using OFSE (refer to Table 3)).

Metric	Metric Weight (1-5)	Porous Media				
		NC Baseline	C	PCC	3D-1	3D-2
Large Range of capillary flow rates	4	0	-1	0	0	0
Selectable capillary flow rate	5	0	0	+1	+1	+1
Uniform wicking front	5	0	0	-1	0	0
High protein binding capacity	4	0	-1	+1	0	0
Effective protein blocking	4	0	0	-1	0	0
High tensile strength	2	0	+1	-1	0	0
Non-collapsing pores and void space	4	0	0	0	0	-1
Wet strength	2	0	+1	0	+1	0
Low extractables/leachables	3	0	0	-1	-1	0
High temperature resistance	3	0	0	-1	0	0
Low/high pH resistance	3	0	0	-1	0	0
Compatible with sample polarities	3	0	0	0	0	+1
Low incidence of surface defects	5	0	-1	0	0	-1
High reproducibility	5	0	-1	-1	0	+1
Choice of dimensions	4	0	0	-1	-1	-1
Low safety risk manufacturing	5	0	+1	+1	+1	+1
Clear display of results	4	0	0	0	0	0
Minimal equipment requirements	4	0	0	0	0	0
Low cost	3	0	+1	+1	-1	-1
<b>TOTAL</b>		<b>0</b>	<b>-6</b>	<b>-7</b>	<b>+2</b>	<b>+1</b>

Considering the technologies overall, PCC based porous media has the most deficiencies in the metrics outlined, and, therefore, the lowest Pugh matrix rating. This suggests that PCC based porous media is not a recommended alternative to nitrocellulose. Where PCC based porous media is proved to be clearly superior to nitrocellulose and other options is in the ease in which capillary flow rate can be controlled, the high protein binding capacity and low manufacturing cost. There are many properties of the calcium carbonate coatings that can be manipulated to achieve the desired wicking rate, and the large specific surface area of PCC allows for many protein binding sites. The prevalence of calcium carbonate as a natural resource, the simple modification chemistry needed to alter its surface, and the low cost of extrusion-based manufacturing makes it a good contender in

lateral flow assay porous media. However, it severely lacks in its chemical compatibility with samples with diverse chemical characteristics, which would be the case for a variety of biological samples. It has also been demonstrated that it is difficult to block calcium carbonate from protein binding meaning the selectivity and specificity of protein-based assays would be compromised. Furthermore, mechanically speaking, PCC coatings are brittle and would depend on backing and casing protection if it ever were to be used in a product. Though little research has been done with regards to other 3D printed materials for lateral flow assays, what does exist does show promise.

## 5 REFERENCES

- [1] S. Sharma, J. Zapatero-Rodríguez, P. Estrela, and R. O’Kennedy, “Point-of-Care diagnostics in low resource settings: Present status and future role of microfluidics,” *Biosensors*, vol. 5, no. 3, pp. 577–601, 2015.
- [2] H. H. Leslie, D. Spiegelman, M. E. Kruk, and H. H. Leslie, “Service readiness of health facilities in Bangladesh, Haiti, Kenya, Malawi, Namibia, Nepal, Rwanda, Senegal, Uganda and the United Republic of Tanzania,” *Bull. World Heal. Organ.*, no. September, pp. 738–748, 2017.
- [3] C. S. Kosack, A. L. Page, and P. R. Klatser, “A guide to aid the selection of diagnostic tests,” *Bull. World Health Organ.*, vol. 95, no. 9, pp. 639–645, 2017.
- [4] E. B. Bahadır and M. K. Sezgintürk, “Lateral flow assays: Principles, designs and labels,” *TrAC - Trends Anal. Chem.*, vol. 82, pp. 286–306, 2016.
- [5] “Rapid Lateral Flow Test Strips- Considerations for Product Development.” EMD Millipore.
- [6] K. M. Koczula and A. Gallotta, “Lateral flow assays,” *Essays Biochem.*, vol. 60, no. 1, pp. 111–120, 2016.
- [7] R. C. Wong and H. Y. Tse, *Lateral Flow Immunoassay*. New York: Humana Press, 2009.
- [8] M. Sajid, A. N. Kawde, and M. Daud, “Designs, formats and applications of lateral flow assay: A literature review,” *J. Saudi Chem. Soc.*, vol. 19, no. 6, pp. 689–705, 2015.
- [9] G. A. Posthuma-Trumpie, J. Korf, and A. Van Amerongen, “Lateral flow (immuno)assay: Its strengths, weaknesses, opportunities and threats. A literature survey,” *Anal. Bioanal. Chem.*, vol. 393, no. 2, pp. 569–582, 2009.
- [10] R. Masoodi *et al.*, *Wicking in Porous Materials- Traditional and Modern Modeling Approaches*. CRC Press, 2013.
- [11] B. M. Cummins, R. Chinthapatla, F. S. Ligler, and G. M. Walker, “Time-Dependent Model for Fluid Flow in Porous Materials with Multiple Pore Sizes,” *Anal. Chem.*, vol. 89, no. 8, pp. 4377–4381, 2017.
- [12] C. L. A. Berli and P. A. Kler, “A quantitative model for lateral flow assays,” *Microfluid. Nanofluidics*, vol. 20, no. 7, pp. 1–9, 2016.
- [13] T. Lappalainen, T. Teerinen, P. Vento, L. Hakalahti, and T. Erho, “Cellulose as a novel substrate for lateral flow assay,” 2010.
- [14] G. E. Fridley, C. A. Holstein, S. B. Oza, and P. Yager, “The evolution of nitrocellulose as a material for bioassays,” *MRS Bull.*, vol. 38, no. 4, pp. 326–330, 2013.
- [15] M. ángeles Fernández de la Ossa, M. López-López, M. Torre, and C. García-Ruiz, “Analytical techniques in the study of highly-nitrated nitrocellulose,” *TrAC - Trends Anal. Chem.*, vol. 30, no. 11, pp. 1740–1755, 2011.
- [16] E. Alinat, N. Delaunay, C. Costanza, X. Archer, and P. Gareil, “Determination of the nitrogen content of nitrocellulose by capillary electrophoresis after alkaline denitration,” *Talanta*, vol. 125, pp. 174–180, 2014.
- [17] S. M. Pourmortazavi, S. G. Hosseini, M. Rahimi-Nasrabadi, S. S. Hajimirsadeghi, and H. Momenian, “Effect of nitrate content on thermal decomposition of nitrocellulose,” *J. Hazard. Mater.*, vol. 162, no. 2–3, pp. 1141–1144, 2009.

- [18] E. J. Flynn, J. Arndt, L. Brothier, and M. A. Morris, “Control of Pore Structure Formation in Cellulose Nitrate Polymer Membranes,” *Adv. Chem. Sci.*, vol. 2, no. 2, 2013.
- [19] K. Hochleitner, “Considerations for membrane selection for lateral flow immunoassays - GE Healthcare Life Sciences,” *GE Healthcare Life Sciences*. [Online]. Available: <https://www.gelifesciences.com/en/us/solutions/lab-filtration/knowledge-center/considerations-for-membrane-selection-for-lateral-flow-immunoassays>. [Accessed: 18-Dec-2019].
- [20] “Nitrocellulose Membrane.” Invitrogen Life Technologies.
- [21] B. A. Baldo, E. R. Tovey, and S. A. Ford, “Comparison of different blocking agents and nitrocellulose in the solid phase detection of proteins by labelled antisera and protein A,” *J. Biochem. Biophys. Methods*, vol. 12, no. 5–6, pp. 271–279, 1986.
- [22] A. L. Ahmad, S. C. Low, S. R. A. Shukor, W. J. N. Fernando, and A. Ismail, “Hindered diffusion in lateral flow nitrocellulose membrane: Experimental and modeling studies,” *J. Memb. Sci.*, vol. 357, no. 1–2, pp. 178–184, 2010.
- [23] A. L. Ahmad, S. C. Low, and S. R. A. Shukor, “Effects of membrane cast thickness on controlling the macrovoid structure in lateral flow nitrocellulose membrane and determination of its characteristics,” *Scr. Mater.*, vol. 57, no. 8, pp. 743–746, 2007.
- [24] W. L. Hung, D. M. Wang, J. Y. Lai, and S. C. Chou, “On the initiation of macrovoids in polymeric membranes - effect of polymer chain entanglement,” *J. Memb. Sci.*, vol. 505, pp. 70–81, 2016.
- [25] “Vivid Lateral Flow Nitrocellulose membranes,” *Pall Corporation*, 2020. [Online]. Available: <https://shop.pall.com/us/en/medical/zidgri78hzq>.
- [26] Merck Millipore, “Hi-Flow Plus Membranes and SureWick Pad Materials,” pp. 1–12, 2017.
- [27] “Hi-Flow Plus.” Millipore Corporation, 2006.
- [28] MDI, “Polyester backed nitrocellulose membrane type CNPH,” p. 1, 2018.
- [29] MDI, “Polyester backed nitrocellulose membrane type CNPF,” p. 1, 2018.
- [30] MDI, “Polyester backed nitrocellulose membrane type CNPC,” p. 1, 2018.
- [31] W. Xiao *et al.*, “A simple and compact smartphone-based device for the quantitative readout of colloidal gold lateral flow immunoassay strips,” *Sensors Actuators, B Chem.*, vol. 266, pp. 63–70, 2018.
- [32] O. Mudanyali, S. Dimitrov, U. Sikora, S. Padmanabhan, I. Navruz, and A. Ozcan, “Integrated rapid-diagnostic-test reader platform on a cellphone,” *Lab Chip*, vol. 12, no. 15, pp. 2678–2686, 2012.
- [33] R. Zou *et al.*, “Up-converting nanoparticle-based immunochromatographic strip for multi-residue detection of three organophosphorus pesticides in food,” *Front. Chem.*, vol. 7, no. FEB, pp. 1–10, 2019.
- [34] E. M. Hamad, G. Hawamdeh, N. A. Jarrad, O. Yasin, S. I. Al-Gharabli, and R. Shadfan, “Detection of Human Chorionic Gonadotropin (hCG) Hormone using Digital Lateral Flow Immunoassay,” *Proc. Annu. Int. Conf. IEEE Eng. Med. Biol. Soc. EMBS*, vol. 2018-July, pp. 3845–3848, 2018.
- [35] A. G. Lalkhen and A. McCluskey, “Clinical tests: Sensitivity and specificity,” *Contin. Educ. Anaesthesia, Crit. Care Pain*, vol. 8, no. 6, pp. 221–223, 2008.
- [36] J. Y. Lichtenberg, Y. Ling, and S. Kim, “Non-specific adsorption reduction methods in biosensing,” *Sensors (Switzerland)*, vol. 19, no. 11, pp. 1–17, 2019.

- [37] K. Mohd Hanafiah, N. Arifin, Y. Bustami, R. Noordin, M. Garcia, and D. Anderson, “Development of Multiplexed Infectious Disease Lateral Flow Assays: Challenges and Opportunities,” *Diagnostics*, vol. 7, no. 3, p. 51, 2017.
- [38] Y. Zhao *et al.*, “Rapid multiplex detection of 10 foodborne pathogens with an up-converting phosphor technology-based 10-channel lateral flow assay,” *Sci. Rep.*, vol. 6, no. January, pp. 1–8, 2016.
- [39] L. D. Tijing, J. R. C. Dizon, I. Ibrahim, A. R. N. Nisay, H. K. Shon, and R. C. Advincula, “3D printing for membrane separation, desalination and water treatment,” *Appl. Mater. Today*, vol. 18, p. 100486, 2020.
- [40] K. V. Wong and A. Hernandez, “A Review of Additive Manufacturing,” *ISRN Mech. Eng.*, vol. 2012, pp. 1–10, 2012.
- [41] H. Dommati, S. S. Ray, J. C. Wang, and S. S. Chen, “A comprehensive review of recent developments in 3D printing technique for ceramic membrane fabrication for water purification,” *RSC Adv.*, vol. 9, no. 29, pp. 16869–16883, 2019.
- [42] Z. Low, Y. T. Chua, B. M. Ray, D. Mattia, I. S. Metcalfe, and D. A. Patterson, “Perspective on 3D printing of separation membranes and comparison to related unconventional fabrication techniques,” *J. Memb. Sci.*, vol. 523, no. October 2016, pp. 596–613, 2017.
- [43] L. Alison *et al.*, “3D printing of sacrificial templates into hierarchical porous materials,” *Sci. Rep.*, vol. 9, no. 1, pp. 1–9, 2019.
- [44] S. S. Ray, H. Dommati, J. C. Wang, and S. S. Chen, “Solvent based Slurry Stereolithography 3D printed hydrophilic ceramic membrane for ultrafiltration application,” *Ceram. Int.*, vol. 46, no. 8, pp. 12480–12488, 2020.
- [45] H. A. Balogun, R. Sulaiman, S. S. Marzouk, A. Giwa, and S. W. Hasan, “3D printing and surface imprinting technologies for water treatment: A review,” *J. Water Process Eng.*, vol. 31, no. October 2018, p. 100786, 2019.
- [46] H. Huang and D. Dean, “3-D printed porous cellulose acetate tissue scaffolds for additive manufacturing,” *Addit. Manuf.*, vol. 31, no. November 2019, p. 100927, 2020.
- [47] M. Asadi-Eydivand, M. Solati-Hashjin, A. Farzad, and N. A. Abu Osman, “Effect of technical parameters on porous structure and strength of 3D printed calcium sulfate prototypes,” *Robot. Comput. Integr. Manuf.*, vol. 37, pp. 57–67, 2016.
- [48] K. Elhattab, P. Sikder, J. M. Walker, M. C. Bottino, and S. B. Bhaduri, “Fabrication and evaluation of 3-D printed PEEK scaffolds containing Macropores by design,” *Mater. Lett.*, vol. 263, p. 127227, 2020.
- [49] A. I. Cernencu *et al.*, “Bioinspired 3D printable pectin-nanocellulose ink formulations,” *Carbohydr. Polym.*, vol. 220, no. January, pp. 12–21, 2019.
- [50] J. Hansson, H. Yasuga, T. Haraldsson, and W. Van Der Wijngaart, “Synthetic microfluidic paper: High surface area and high porosity polymer micropillar arrays,” *Lab Chip*, vol. 16, no. 2, pp. 298–304, 2016.
- [51] E. Jutila, R. Koivunen, and P. Gane, “Effect of coating pigment, binder type and binder amount on planar liquid wicking on coated substrates,” *J. Print Media Technol. Res.*, vol. 4, no. 3, pp. 173–186, 2015.
- [52] R. Koivunen, E. Jutila, R. Bollström, and P. Gane, “Hydrophobic patterning of functional porous pigment coatings by inkjet printing,” *Microfluid. Nanofluidics*, vol. 20, no. 6, pp. 1–21, 2016.

- [53] E. Jutila, R. Koivunen, I. Kiiski, R. Bollström, T. Sikanen, and P. Gane, “Microfluidic Lateral Flow Cytochrome P450 Assay on a Novel Printed Functionalized Calcium Carbonate-Based Platform for Rapid Screening of Human Xenobiotic Metabolism,” *Adv. Funct. Mater.*, vol. 28, no. 31, pp. 1–11, 2018.
- [54] E. Jutila, R. Koivunen, R. Bollström, and P. Gane, “Wicking and chromatographic properties of highly porous functionalised calcium carbonate coatings custom-designed for microfluidic devices,” *J. Micromechanics Microengineering*, vol. 29, no. 5, 2019.
- [55] L. Brečević and D. Kralj, “On calcium carbonates: From fundamental research to application,” *Croat. Chem. Acta*, vol. 80, no. 3–4, pp. 467–484, 2007.
- [56] E. M. Flaten, M. Seiersten, and J. P. Andreassen, “Polymorphism and morphology of calcium carbonate precipitated in mixed solvents of ethylene glycol and water,” *J. Cryst. Growth*, vol. 311, no. 13, pp. 3533–3538, 2009.
- [57] S. R. Dickinson and K. M. McGrath, “Quantitative determination of binary and tertiary calcium carbonate mixtures using powder X-ray diffraction,” *Analyst*, vol. 126, no. 7, pp. 1118–1121, 2001.
- [58] N. Erdogan and H. A. Eken, “Precipitated Calcium carbonate production, synthesis and properties,” *Physicochem. Probl. Miner. Process.*, vol. 53, no. 1, pp. 57–68, 2017.
- [59] P. Somasundaran and G. E. Agar, “The zero point of charge of calcite,” *J. Colloid Interface Sci.*, vol. 24, no. 4, pp. 433–440, 1967.
- [60] O. A. Jimoh, K. S. Ariffin, H. Bin Hussin, and A. E. Temitope, “Synthesis of precipitated calcium carbonate: a review,” *Carbonates and Evaporites*, vol. 33, no. 2, pp. 331–346, 2018.
- [61] “Precipitated Calcium Carbonate,” *Specialty Minerals*. [Online]. Available: [https://www.mineralstech.com/business-segments/specialty-minerals/paper-pcc/precipitated-calcium-carbonate-\(pcc\)](https://www.mineralstech.com/business-segments/specialty-minerals/paper-pcc/precipitated-calcium-carbonate-(pcc)).
- [62] C. L. Levy *et al.*, “Diffusion and Tortuosity in Porous Functionalized Calcium Carbonate,” *Ind. Eng. Chem. Res.*, vol. 54, no. 41, pp. 9938–9947, 2015.
- [63] “Omyamatt Modified Calcium Carbonates as matting agents for emulsion paints.” Omya Inc., 2019.
- [64] Y. Li, L. Tran, C. D. M. Filipe, J. D. Brennan, and R. H. Pelton, “Printed Thin Films with Controlled Porosity as Lateral Flow Media,” 2019.
- [65] A. Shrivastava, *Introduction to Plastics Engineering*. Elsevier, 2018.
- [66] M. Kaplan, “Alkaline Phosphatase,” *Gastroenterology*, vol. 62, no. 3, p. 1972, 1972.
- [67] J. S. Clark and R. C. Turner, “Reactions Between Solid Calcium Carbonate and Orthophosphate Solutions,” *Can. J. Chem.*, vol. 33, no. 4, pp. 665–671, 1955.
- [68] J. Schoelkopf, P. A. C. Gane, C. J. Ridgway, and G. P. Matthews, “Practical observation of deviation from Lucas-Washburn scaling in porous media,” *Colloids Surfaces A Physicochem. Eng. Asp.*, vol. 206, no. 1–3, pp. 445–454, 2002.
- [69] C. J. Ridgway, P. A. C. Gane, and J. Schoelkopf, “Modified calcium carbonate coatings with rapid absorption and extensive liquid uptake capacity,” *Colloids Surfaces A Physicochem. Eng. Asp.*, vol. 236, no. 1–3, pp. 91–102, 2004.
- [70] C. J. Ridgway, P. A. C. Gane, and J. Schoelkopf, “Achieving rapid absorption and extensive liquid uptake capacity in porous structures by decoupling capillarity and permeability: Nanoporous modified calcium carbonate,” *Transp. Porous Media*, vol. 63, no. 2, pp. 239–259, 2006.

- [71] G. T. Nolan, “Computer Simulation of Random Packings of Hard Spheres,” *Powder Technol.*, vol. 62, pp. 189–196, 1990.
- [72] P. A. Gane, J. P. Kettle, G. P. Matthews, and C. J. Ridgway, “Void space structure of compressible polymer spheres and consolidated calcium carbonate paper-coating formulations,” *Ind. Eng. Chem. Res.*, vol. 35, no. 5, pp. 1753–1764, 1996.
- [73] M. Guvendiren, A. Soshinski, R. Gambogi, and S. Yang, “Calcium Carbonate Composite Hydrogel Films: Particle Packing and Optical Properties,” *Polym. Eng. Sci.*, 2012.
- [74] *Surface Coatings*. Oil and Colour Chemists’ Association, 1983.
- [75] A. Goldschmidt and H.-J. Streintberger, *Basics of Coating Technology*. Hannover: BASF Coatings AG, 2003.
- [76] C. C. Roberts and L. F. Francis, “Drying and cracking of soft latex coatings,” *J. Coatings Technol. Res.*, vol. 10, no. 4, pp. 441–451, 2013.
- [77] “Dispersions for Adhesives and Construction.” BASF BTC Chemical Distribution.
- [78] J. R. Choi, J. Hu, S. Feng, W. A. B. Wan Abas, B. Pinguan-Murphy, and F. Xu, “Sensitive biomolecule detection in lateral flow assay with a portable temperature-humidity control device,” *Biosens. Bioelectron.*, vol. 79, pp. 98–107, 2016.
- [79] “Omyamatt® 75 - ME.” Omya International, Oftringen, p. 51934, 2019.
- [80] D. S. Horne, “Casein structure, self-assembly and gelation,” *Curr. Opin. Colloid Interface Sci.*, vol. 7, no. 5–6, pp. 456–461, 2002.
- [81] C. Broyard and F. Gaucheron, “Modifications of structures and functions of caseins: a scientific and technological challenge,” *Dairy Sci. Technol.*, vol. 95, no. 6, pp. 831–862, 2015.
- [82] C. Holt and L. Sawyer, “Caseins as rheomorphic proteins: Interpretation of primary and secondary structures of the  $\alpha$ s1-,  $\beta$ - and  $\kappa$ -caseins,” *J. Chem. Soc. Faraday Trans.*, vol. 89, no. 15, pp. 2683–2692, 1993.
- [83] M. Glantz, T. G. Devold, G. E. Vegarud, H. Lindmark Månsson, H. Stålhammar, and M. Paulsson, “Importance of casein micelle size and milk composition for milk gelation,” *J. Dairy Sci.*, vol. 93, no. 4, pp. 1444–1451, 2010.
- [84] H. Breiteneder and E. N. C. Mills, “Molecular properties of food allergens,” *J. Allergy Clin. Immunol.*, vol. 115, no. 1, pp. 14–23, 2005.
- [85] “Casein from bovine milk Product Information.” Sigma-Aldrich Inc., 2006.
- [86] K. A. Majorek *et al.*, “Structural and immunologic characterization of bovine, horse, and rabbit serum albumins,” vol. 52, pp. 174–182, 2013.
- [87] S. C. Low, R. Shaimi, Y. Thandaithabany, J. K. Lim, A. L. Ahmad, and A. Ismail, “Electrophoretic interactions between nitrocellulose membranes and proteins: Biointerface analysis and protein adhesion properties,” *Colloids Surfaces B Biointerfaces*, vol. 110, pp. 248–253, 2013.
- [88] H. T. M. Phan, S. Bartelt-Hunt, K. B. Rodenhausen, M. Schubert, and J. C. Bartz, “Investigation of bovine serum albumin (BSA) attachment onto self-assembled monolayers (SAMs) using combinatorial quartz crystal microbalance with dissipation (QCM-D) and spectroscopic ellipsometry (SE),” *PLoS One*, vol. 10, no. 10, 2015.
- [89] Y. Avnimelech, “Calcium-carbonate-phosphate surface complex in calcareous systems,” *Nature*, vol.

288, no. November, pp. 255–256, 1980.

- [90] Z. Li *et al.*, “Phosphate adsorption and precipitation on calcite under calco-carbonic equilibrium condition,” *Chemosphere*, vol. 183, pp. 419–428, 2017.
- [91] M. Mosquet, Y. Chevalier, S. Brunel, J. P. Guicquero, and P. Le Perhec, “Polyoxyethylene di-phosphonates as efficient dispersing polymers for aqueous suspensions,” *J. Appl. Polym. Sci.*, vol. 65, no. 12, pp. 2545–2555, 1997.
- [92] P. T. Charles, V. R. Stubbs, C. M. Soto, B. D. Martin, B. J. White, and C. R. Taitt, “Reduction of non-specific protein adsorption using poly(ethylene) glycol (PEG) modified polyacrylate hydrogels in immunoassays for staphylococcal enterotoxin B detection,” *Sensors*, vol. 9, no. 1, pp. 645–655, 2009.
- [93] “Methoxy PEG Phosphate,” *JenKem Technology USA*. [Online]. Available: <https://www.jenkemusa.com/product/methoxy-peg-phos>.